Electronic Supporting Information (ESI) for:

Homoleptic ruthenium(II) complexes bearing imidazol(in)ium-2-dithiocarboxylate ligands: synthesis, characterization, and redox properties

Valdemiro P. Carvalho Jr,[‡a] Guillermo Zaragoza[b] and Lionel Delaude*[a]

[a]Laboratory of Organometallic Chemistry and Homogeneous Catalysis, Institut de chimie (B6a), Allée du six Août 13, Quartier Agora, Université de Liège, 4000 Liège, Belgium.
E-mail: l.delaude@uliege.be; http://www.cata.ulg.ac.be

[b]Unidade de Difracción de Raios X, Edificio CACTUS, Universidade de Santiago de Compostela, Campus Vida, 15782 Santiago de Compostela, Spain

[‡]Present address: Faculdade de Ciências e Tecnologia, UNESP – Univ. Estadual Paulista, Presidente Prudente, SP, Brazil.

Table of content

Part 1 – NMR spectra

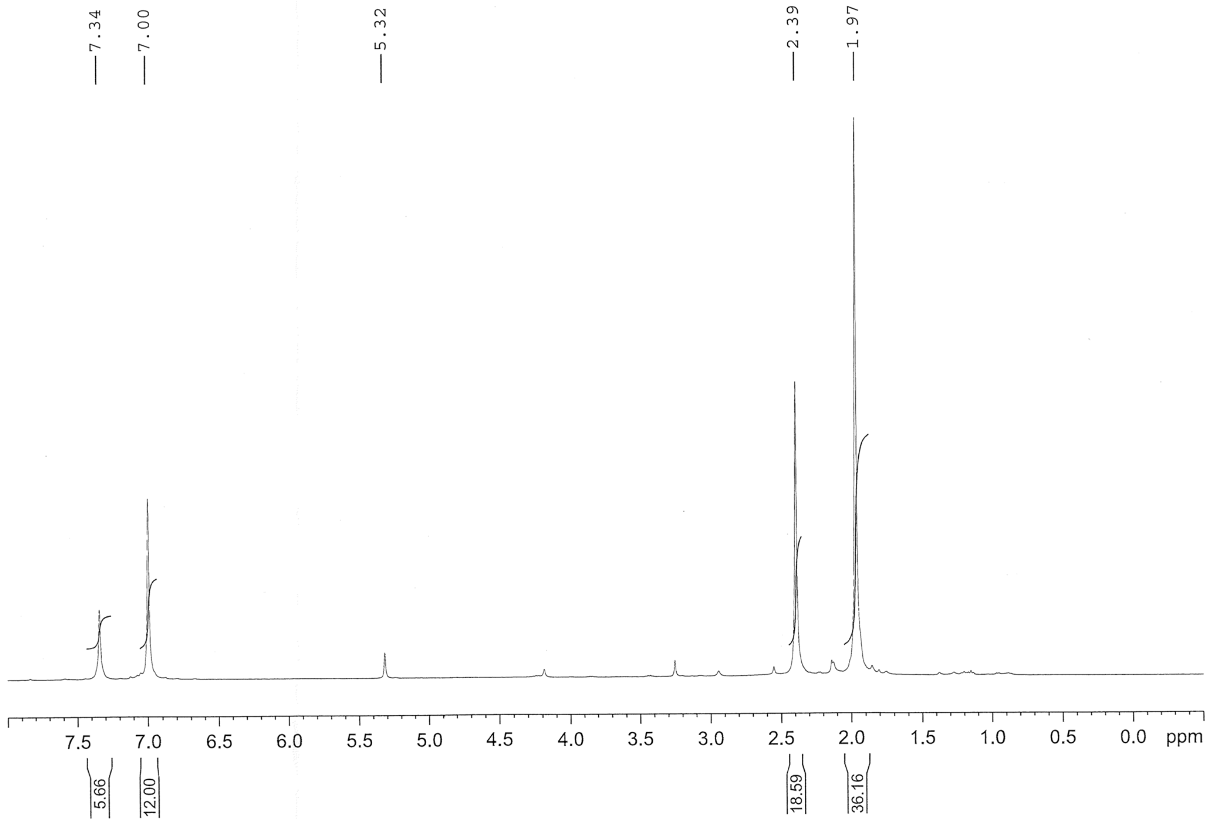

Fig. S1. ^{1}H NMR spectrum (400 MHz, CD_2Cl_2, 298 K) of $[Ru(S_2C{\cdot}IMes)_3](PF_6)_2$ (**2a**)

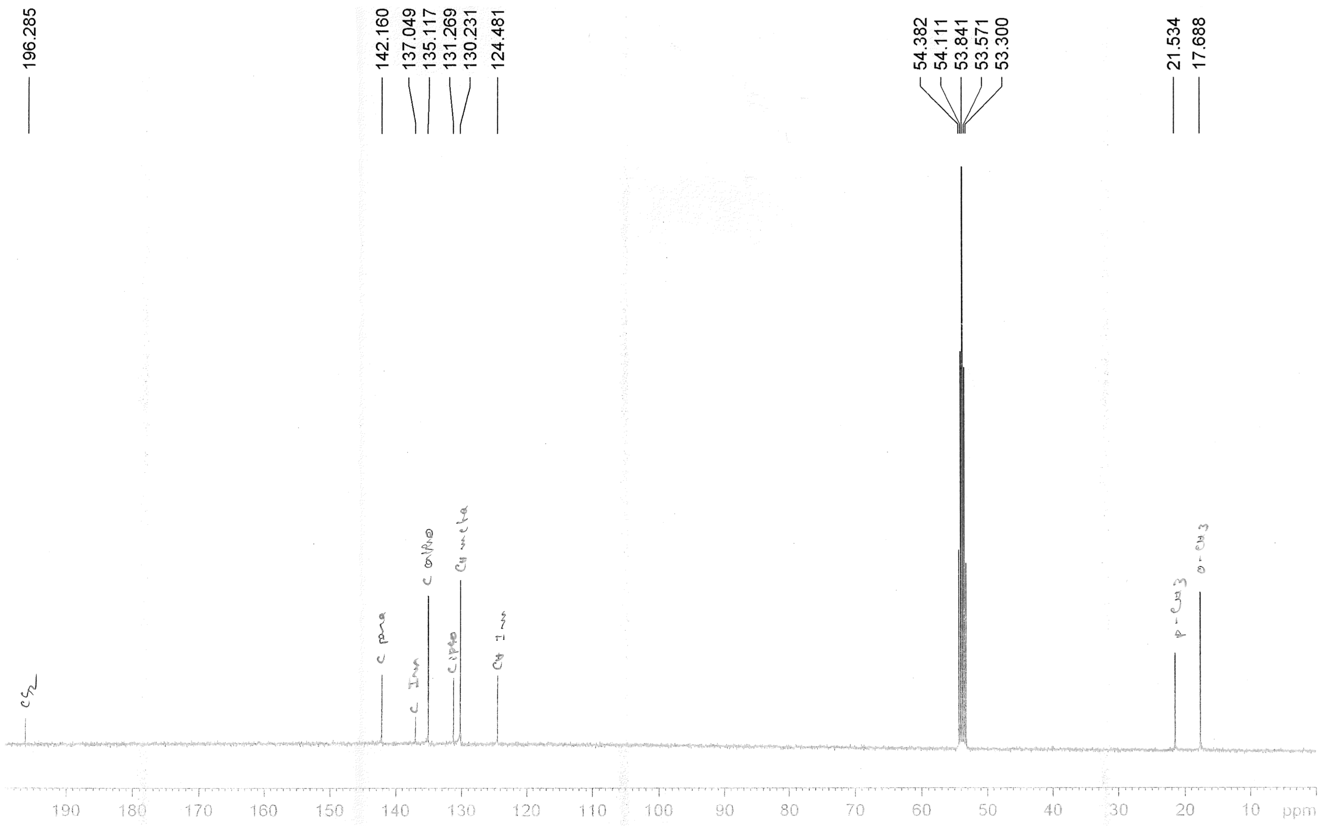

Fig. S2. $^{13}C\{^{1}H\}$ NMR spectrum (101 MHz, CD_2Cl_2, 298 K) of $[Ru(S_2C{\cdot}IMes)_3](PF_6)_2$ (**2a**)

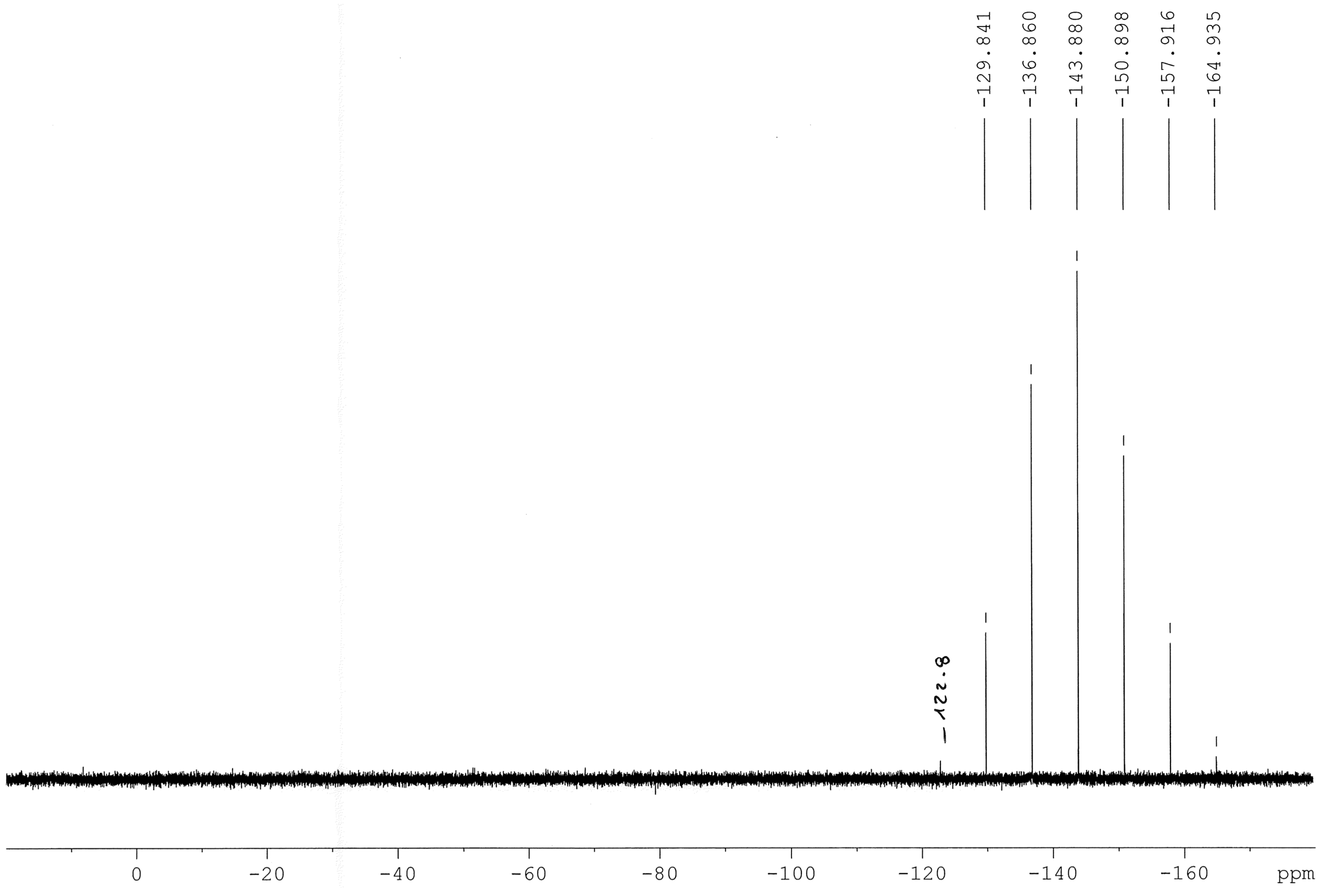

Fig. S3. ^{31}P NMR spectrum (101 MHz, CD_2Cl_2, 298 K) of $[Ru(S_2C{\cdot}IMes)_3](PF_6)_2$ (**2a**)

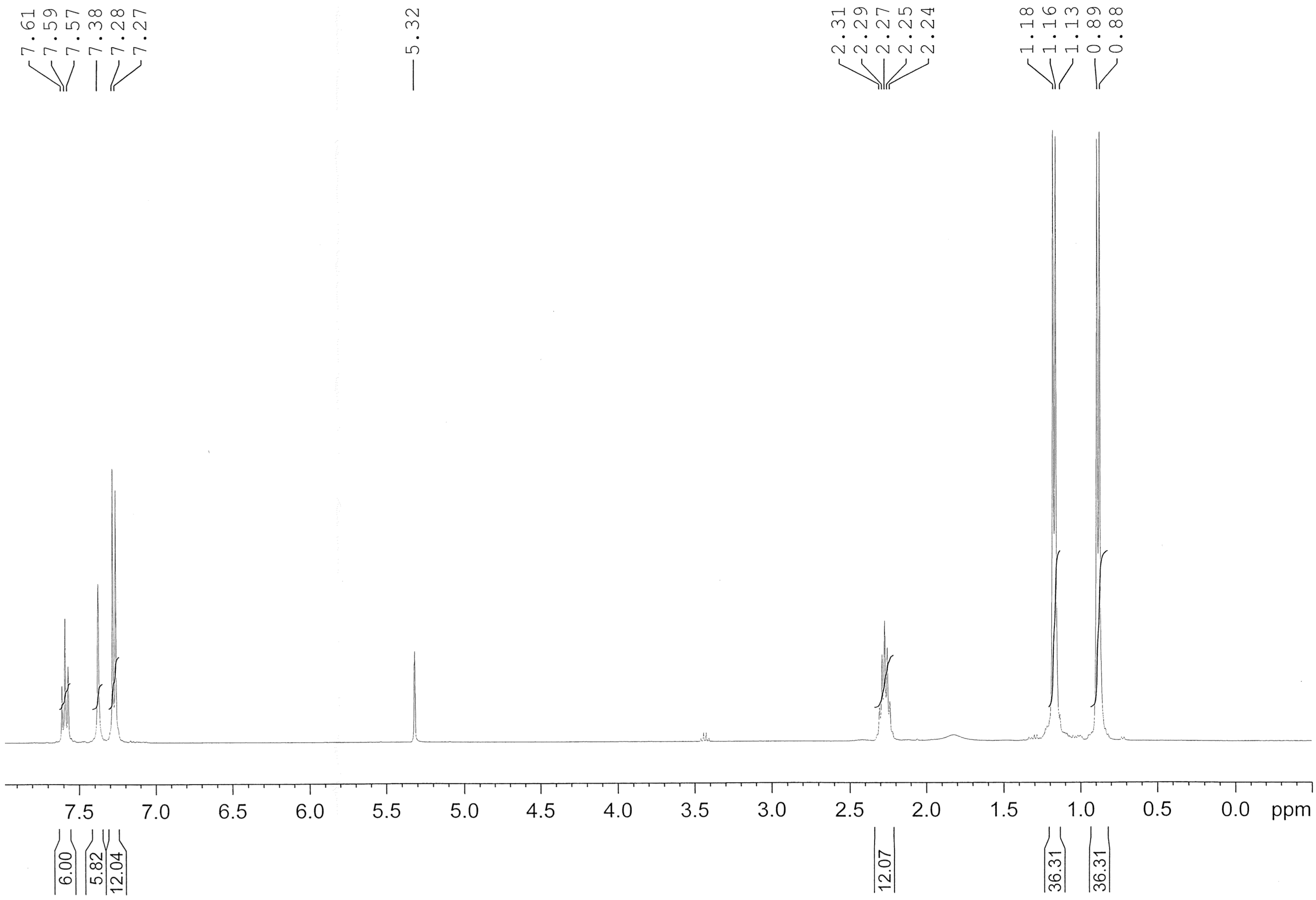

Fig. S4. ^{1}H NMR spectrum (400 MHz, CD_2Cl_2, 298 K) of $[Ru(S_2C \cdot IDip)_3](PF_6)_2$ (**2b**)

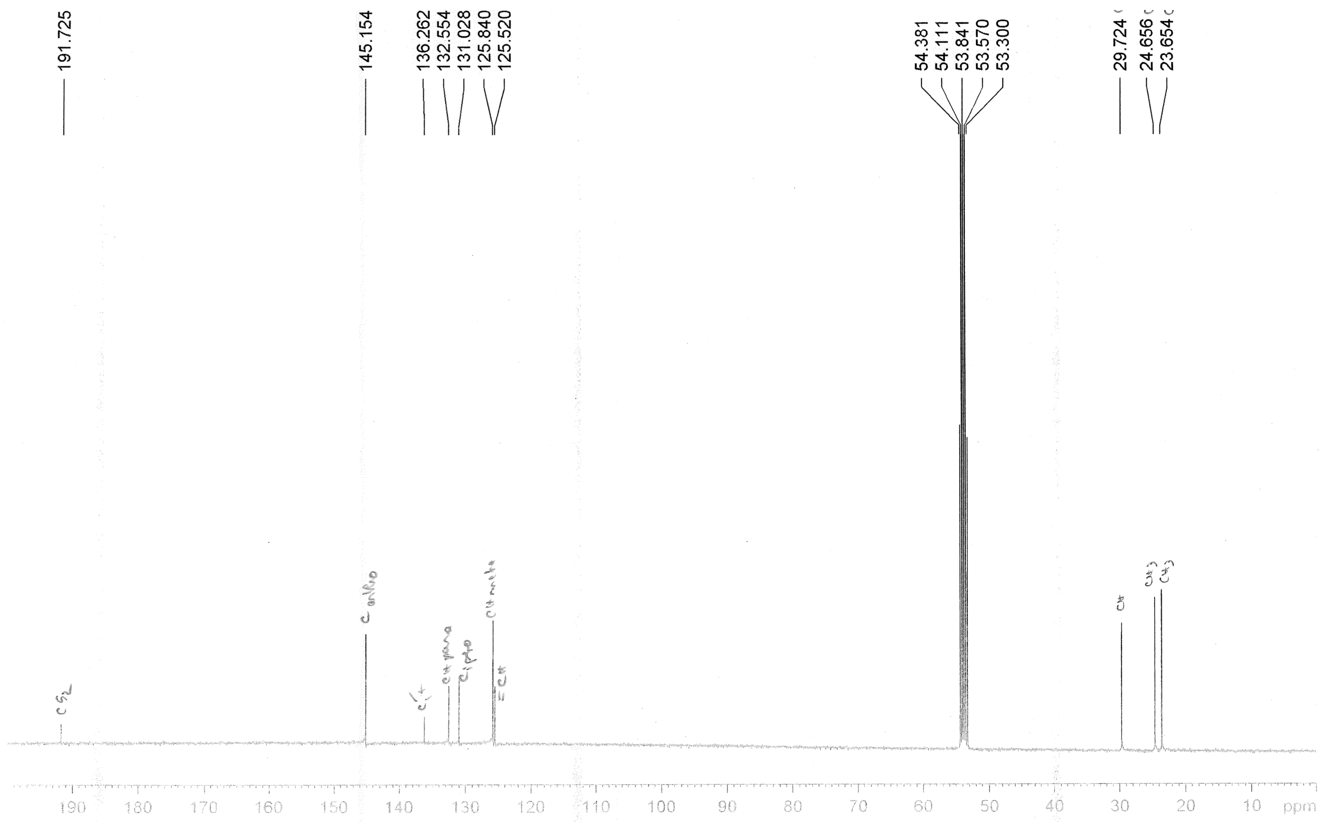

Fig. S5. $^{13}C\{^{1}H\}$ NMR spectrum (101 MHz, CD_2Cl_2, 298 K) of $[Ru(S_2C \cdot IDip)_3](PF_6)_2$ (**2b**)

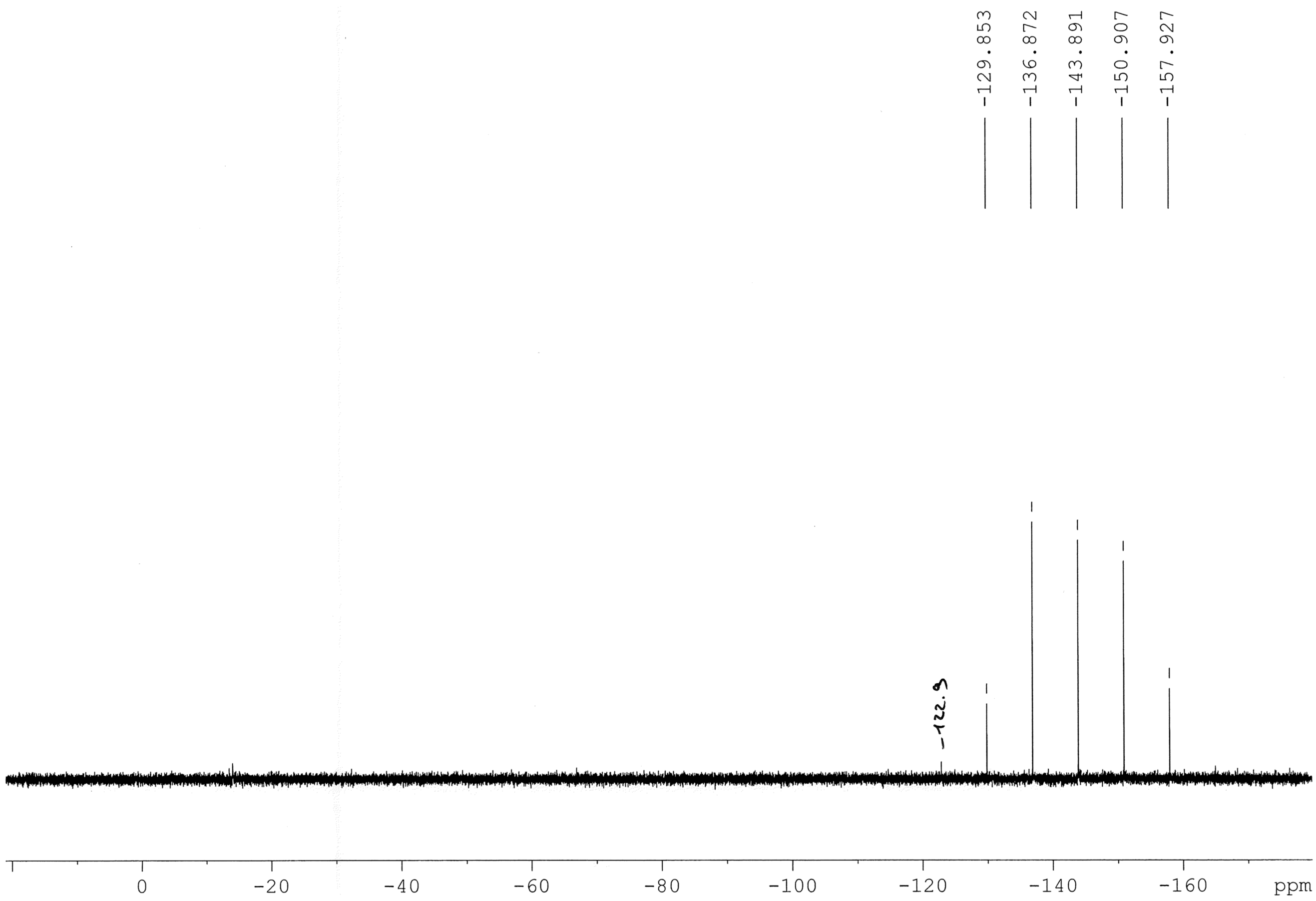

Fig. S6. ^{31}P NMR spectrum (101 MHz, CD_2Cl_2, 298 K) of $[Ru(S_2C{\cdot}IDip)_3](PF_6)_2$ (**2b**)

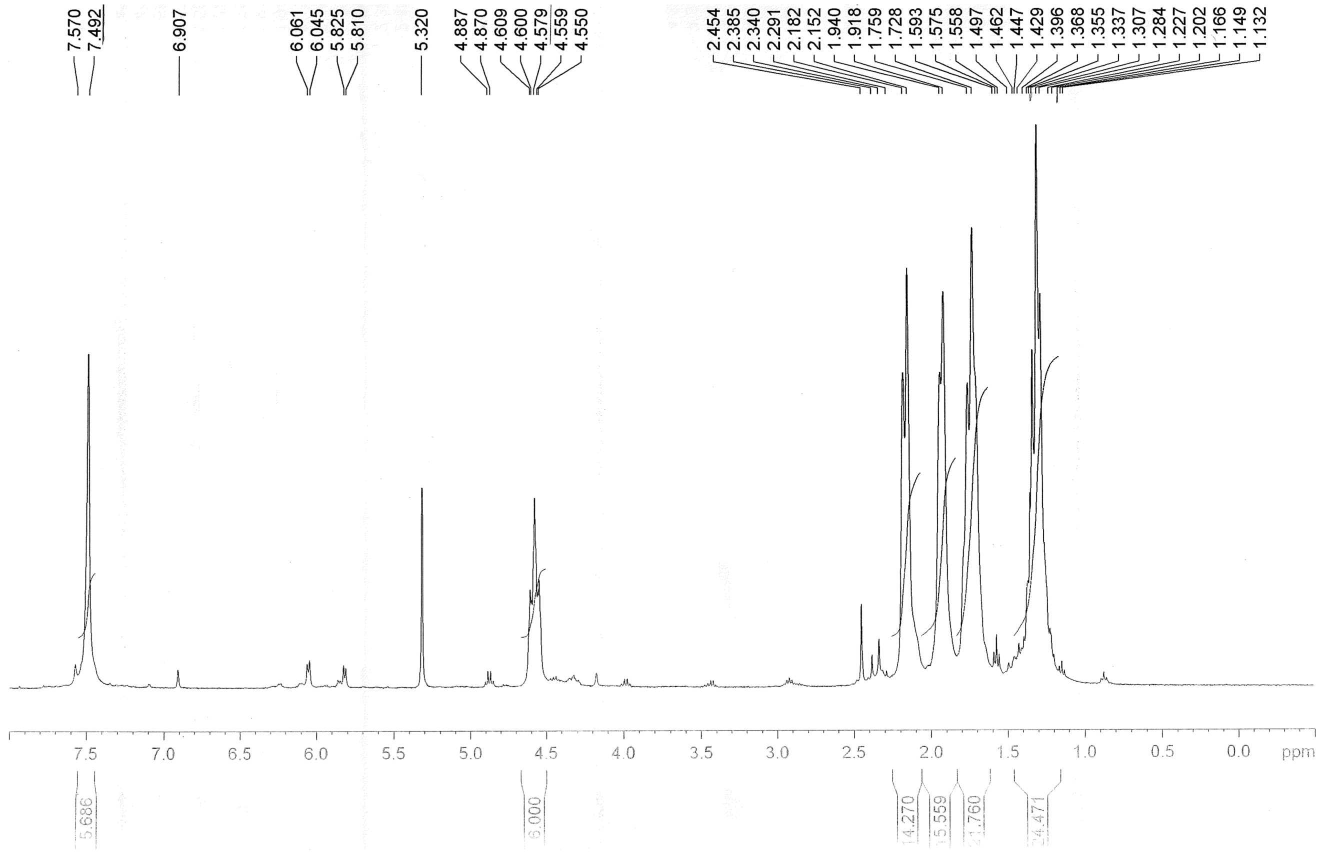

Fig. S7. ^{1}H NMR spectrum (400 MHz, CD_2Cl_2, 298 K) of $[Ru(S_2C{\cdot}ICy)_3](PF_6)_2$ (**2c**)

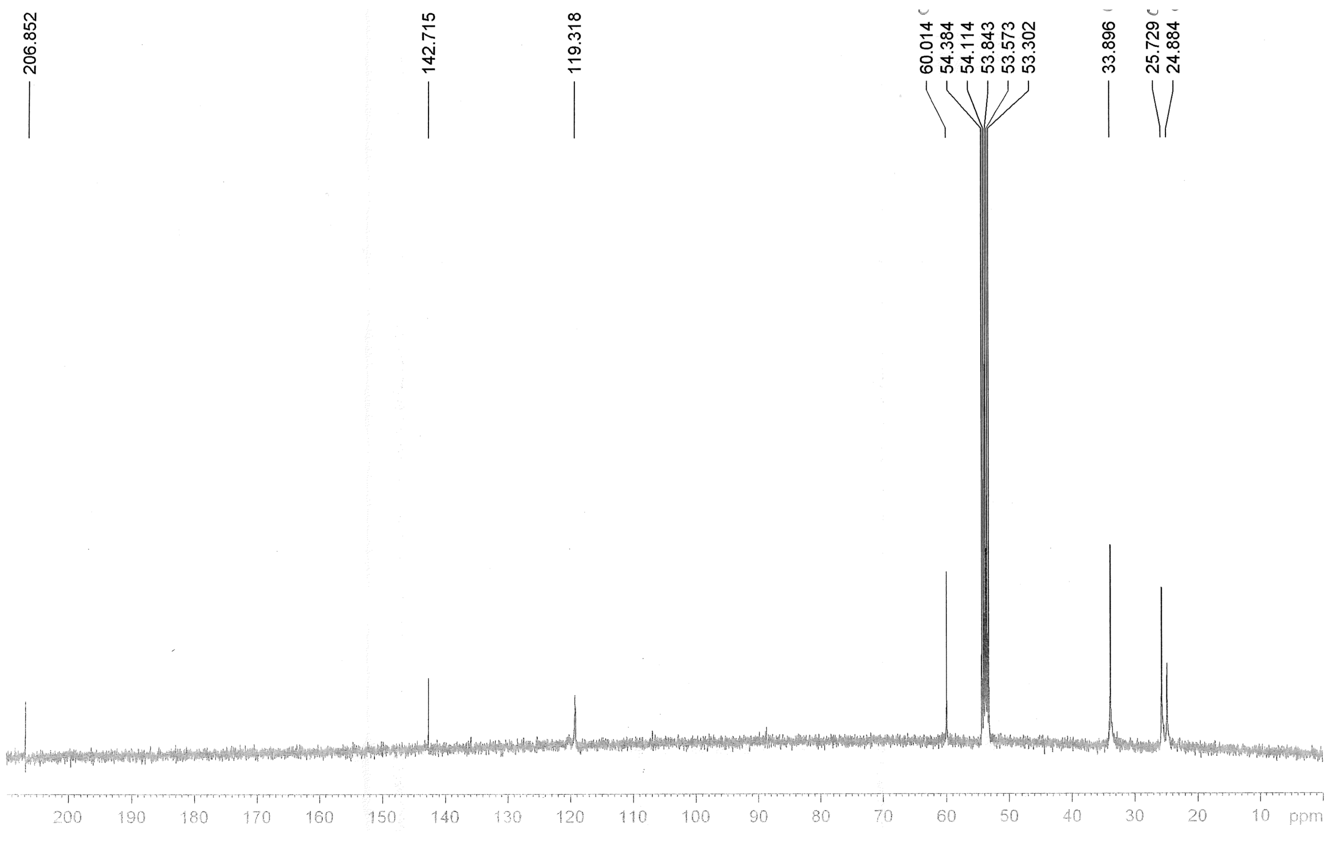

Fig. S8. $^{13}C\{^{1}H\}$ NMR spectrum (101 MHz, CD_2Cl_2, 298 K) of $[Ru(S_2C{\cdot}ICy)_3](PF_6)_2$ (**2c**)

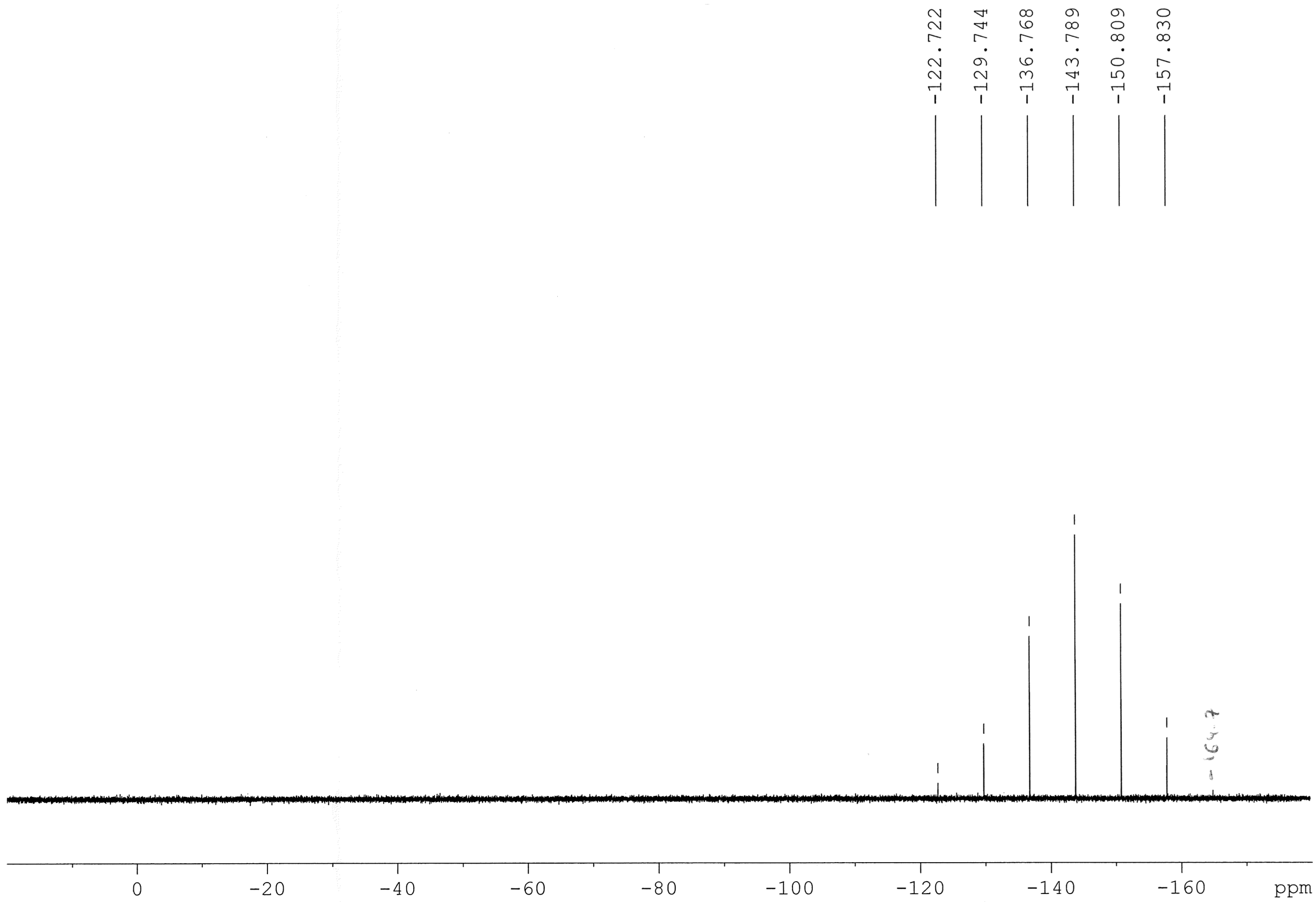

Fig. S9. ^{31}P NMR spectrum (101 MHz, CD_2Cl_2, 298 K) of $[Ru(S_2C{\cdot}ICy)_3](PF_6)_2$ (**2c**)

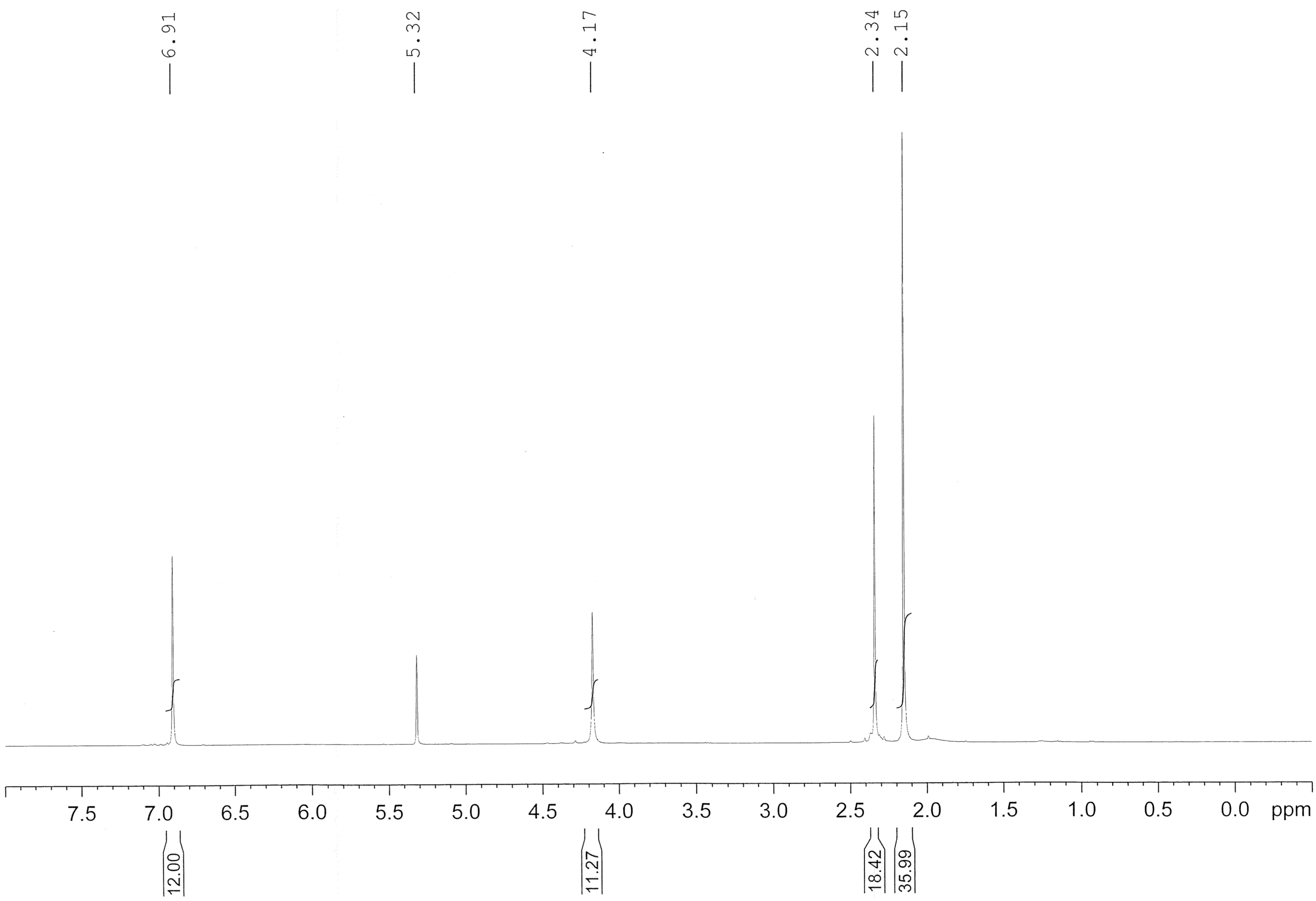

Fig. S10. ^{1}H NMR spectrum (400 MHz, CD_2Cl_2, 298 K) of $[Ru(S_2C\cdot SIMes)_3](PF_6)_2$ (**2d**)

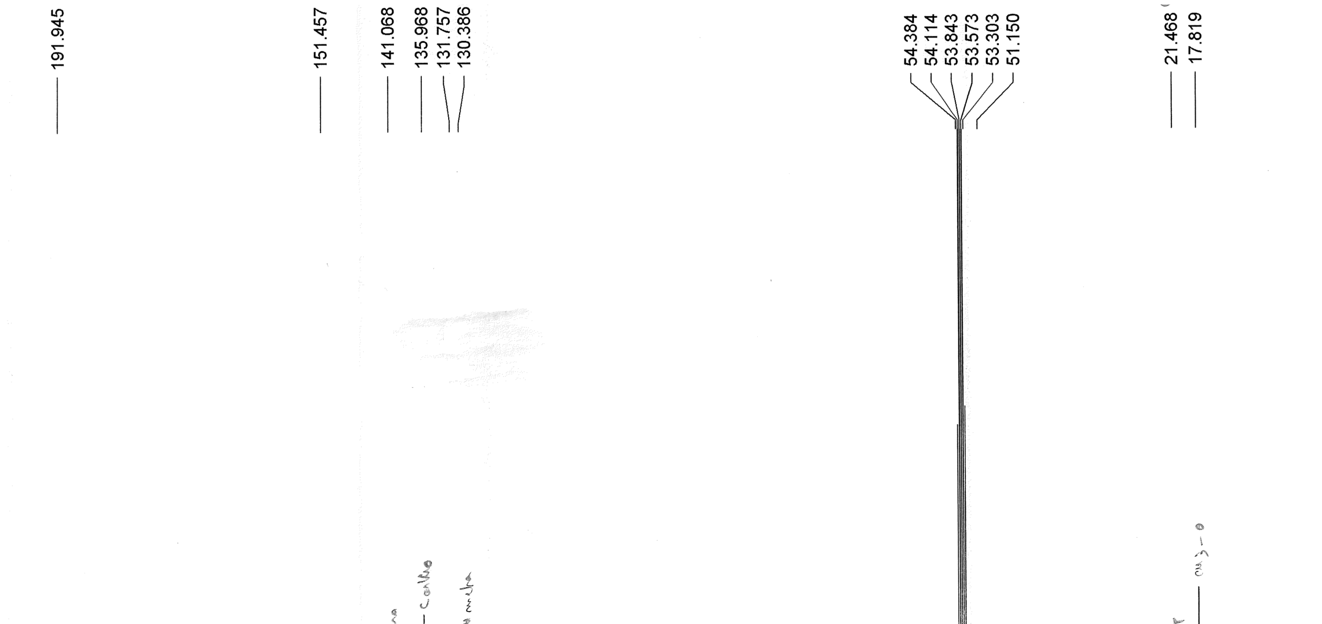

Fig. S11. $^{13}C\{^{1}H\}$ NMR spectrum (101 MHz, CD_2Cl_2, 298 K) of $[Ru(S_2C\cdot SIMes)_3](PF_6)_2$ (**2d**)

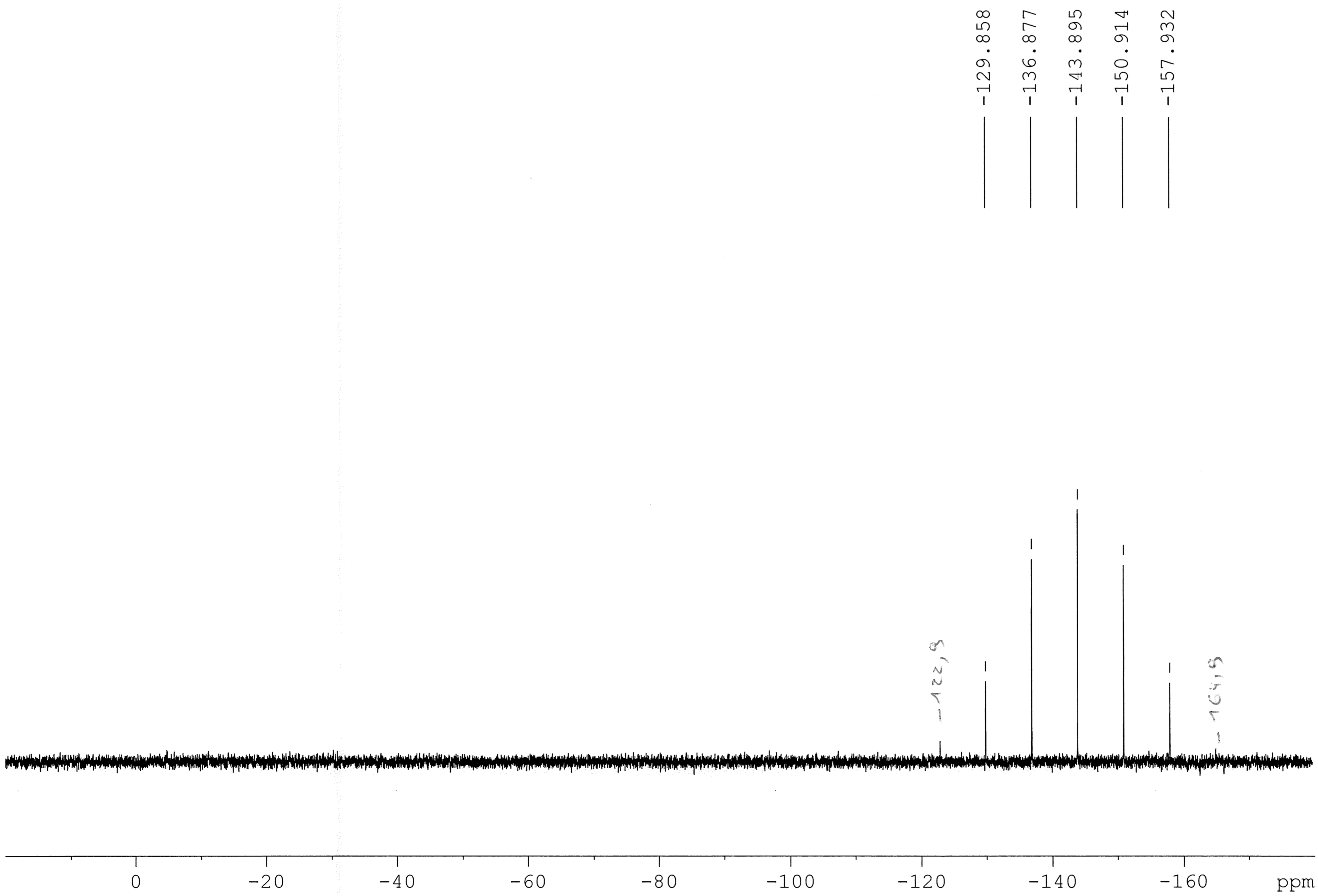

Fig. S12. ^{31}P NMR spectrum (101 MHz, CD_2Cl_2, 298 K) of $[Ru(S_2C{\cdot}SIMes)_3](PF_6)_2$ (**2d**)

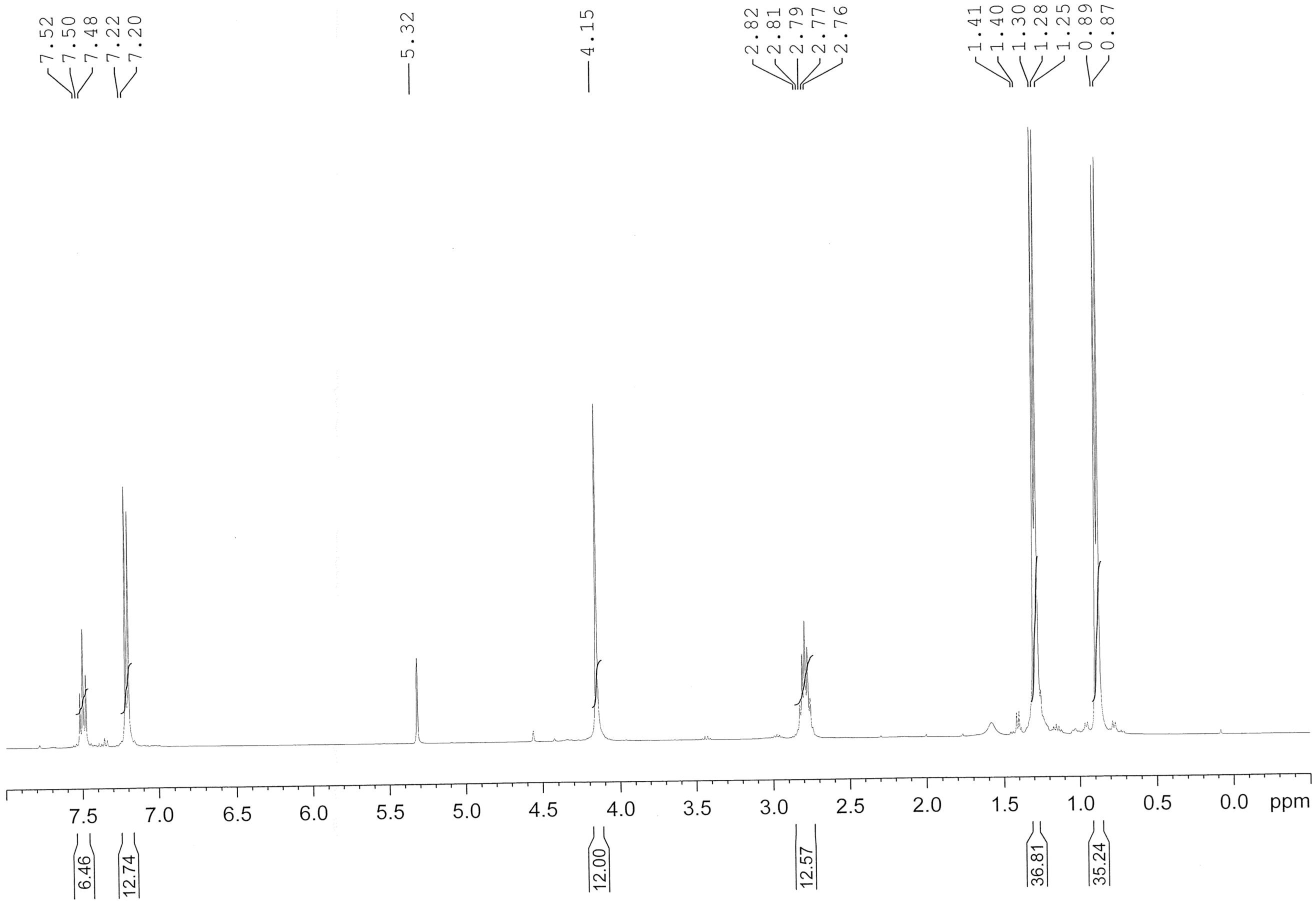

Fig. S13. ^{1}H NMR spectrum (400 MHz, CD_2Cl_2, 298 K) of $[Ru(S_2C{\cdot}SIDip)_3](PF_6)_2$ (**2e**)

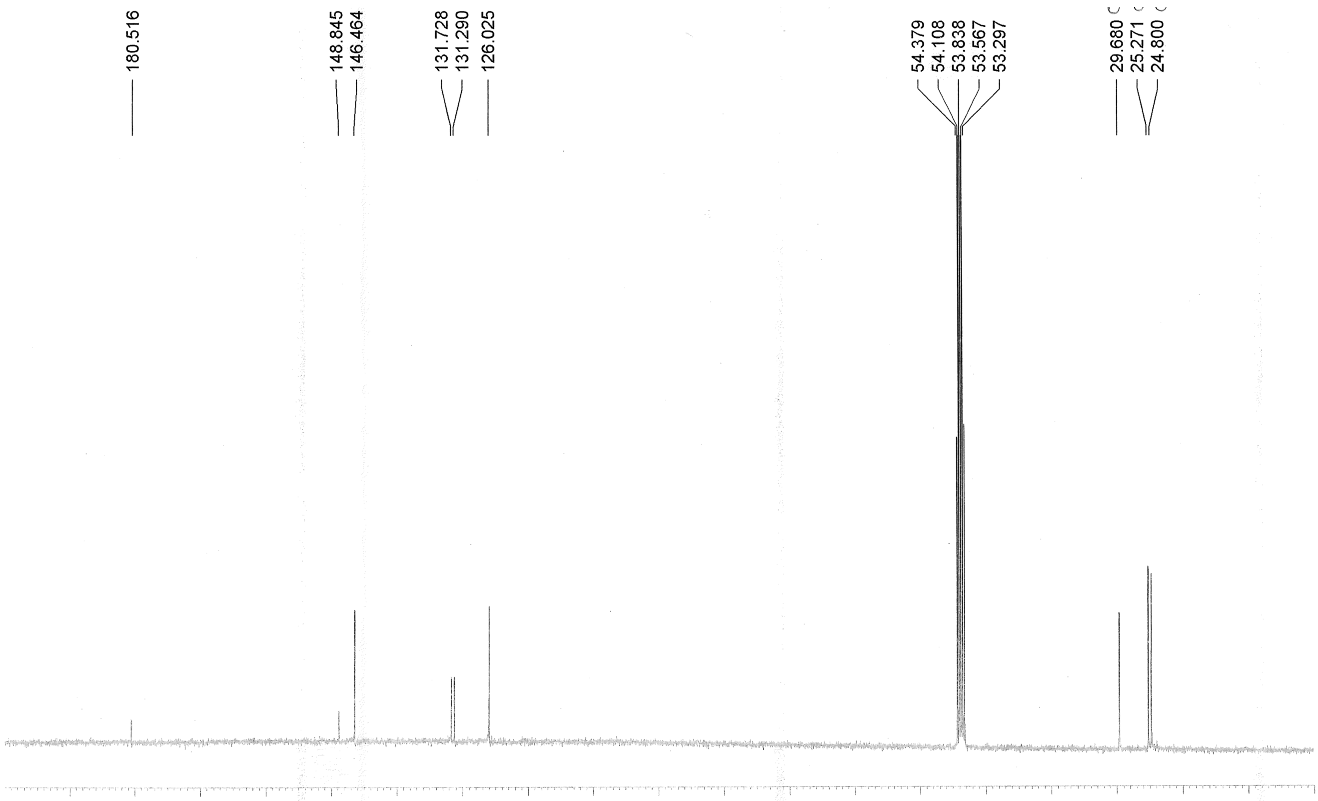

Fig. S14. $^{13}C\{^1H\}$ NMR spectrum (101 MHz, CD_2Cl_2, 298 K) of $[Ru(S_2C{\cdot}SIDip)_3](PF_6)_2$ (**2e**)

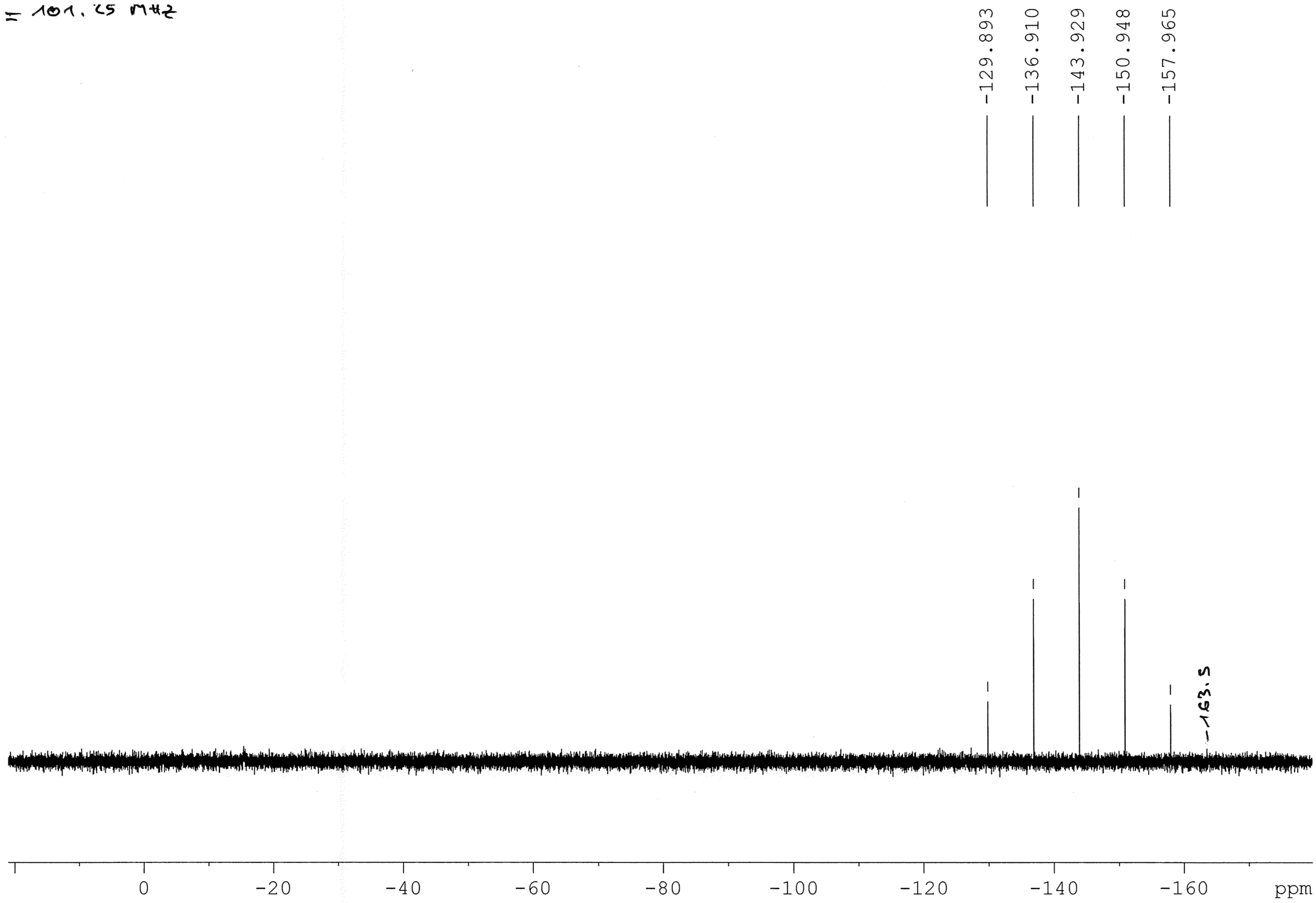

Fig. S15. ^{31}P NMR spectrum (101 MHz, CD_2Cl_2, 298 K) of $[Ru(S_2C\cdot SIDip)_3](PF_6)_2$ (**2e**)

Part 2 – IR spectra

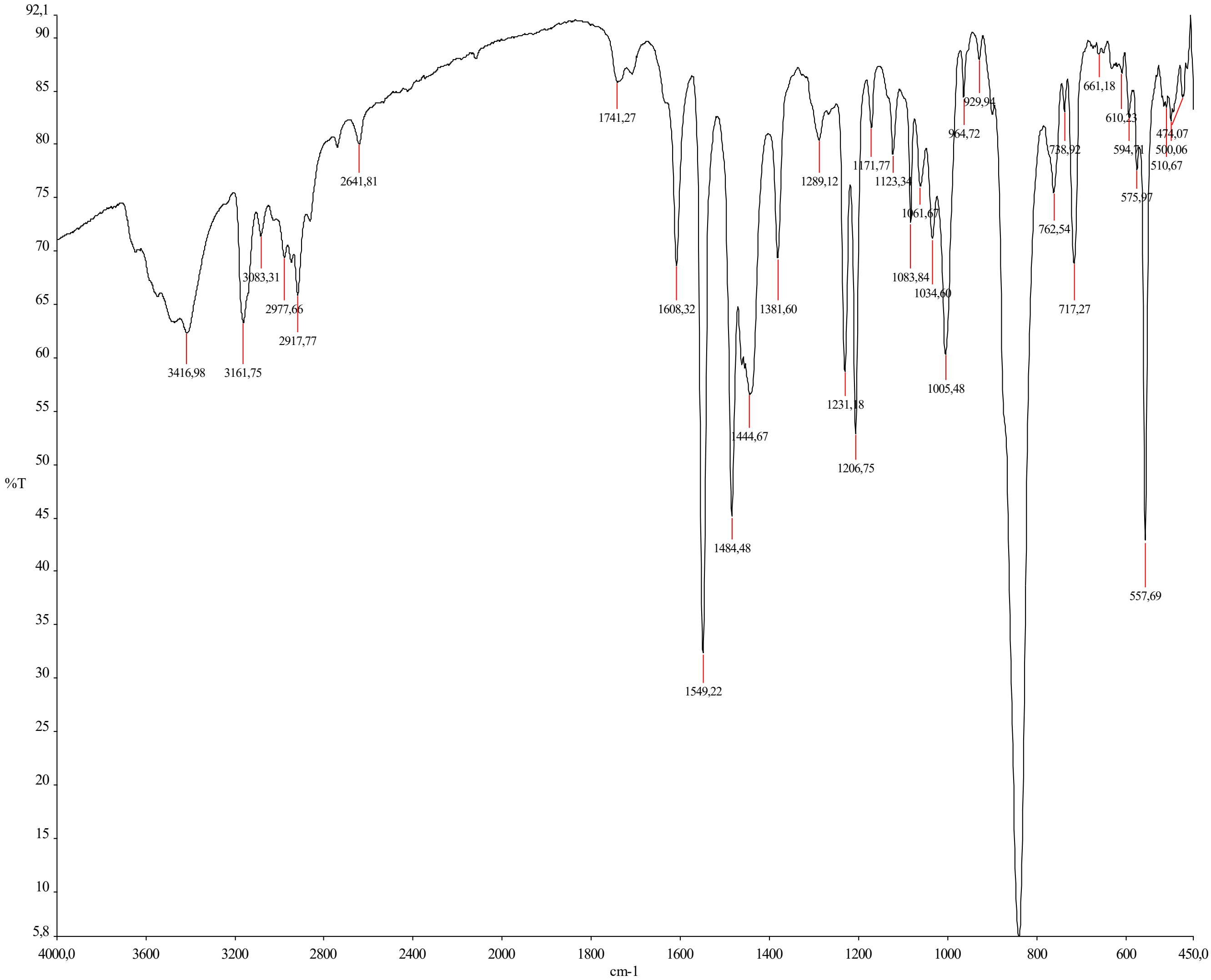

Fig. S16. FT-IR spectrum (KBr) of $[Ru(S_2C{\cdot}IMes)_3](PF_6)_2$ (**2a**)

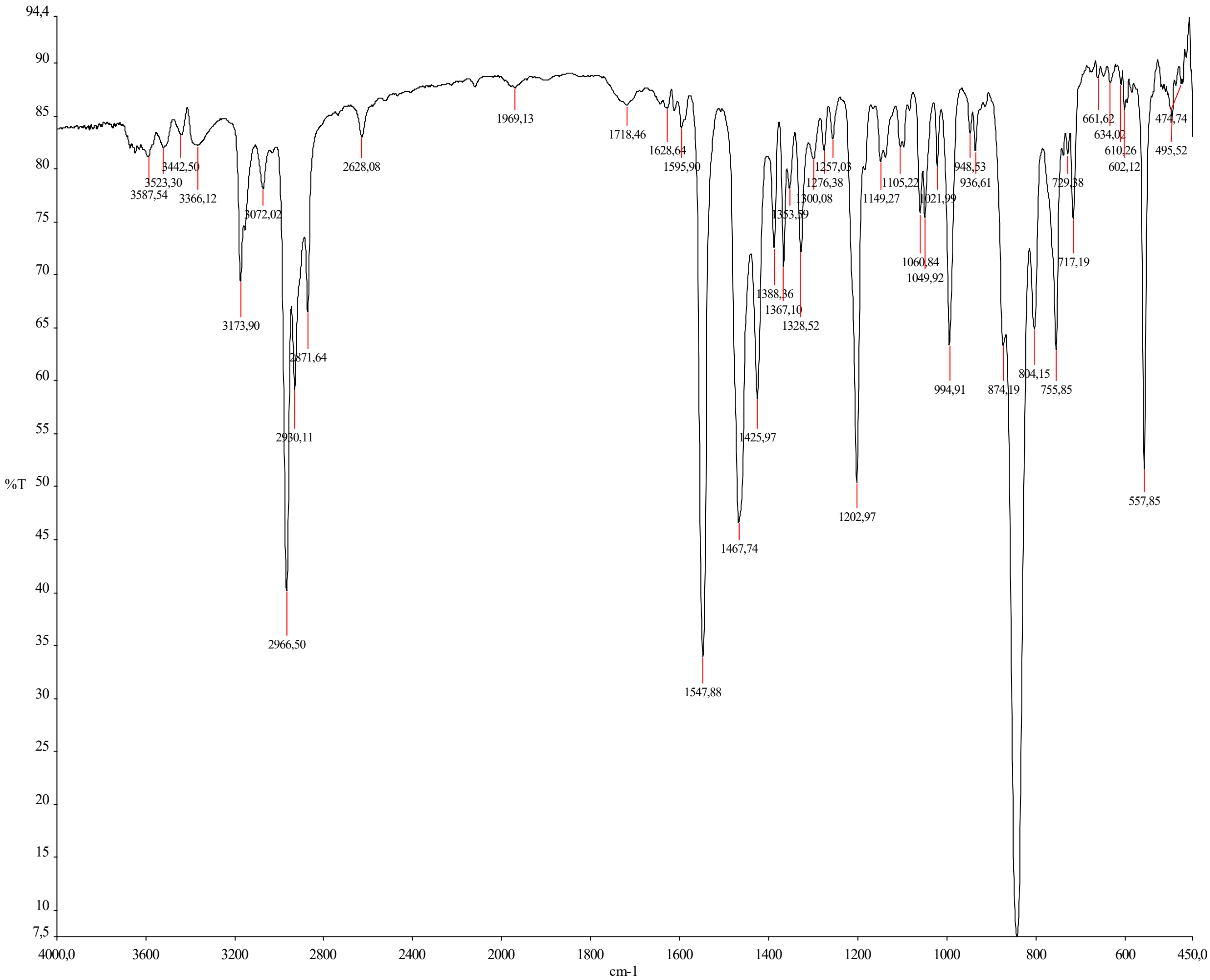

Fig. S17. FT-IR spectrum (KBr) of $[Ru(S_2C{\cdot}IDip)_3](PF_6)_2$ (**2b**)

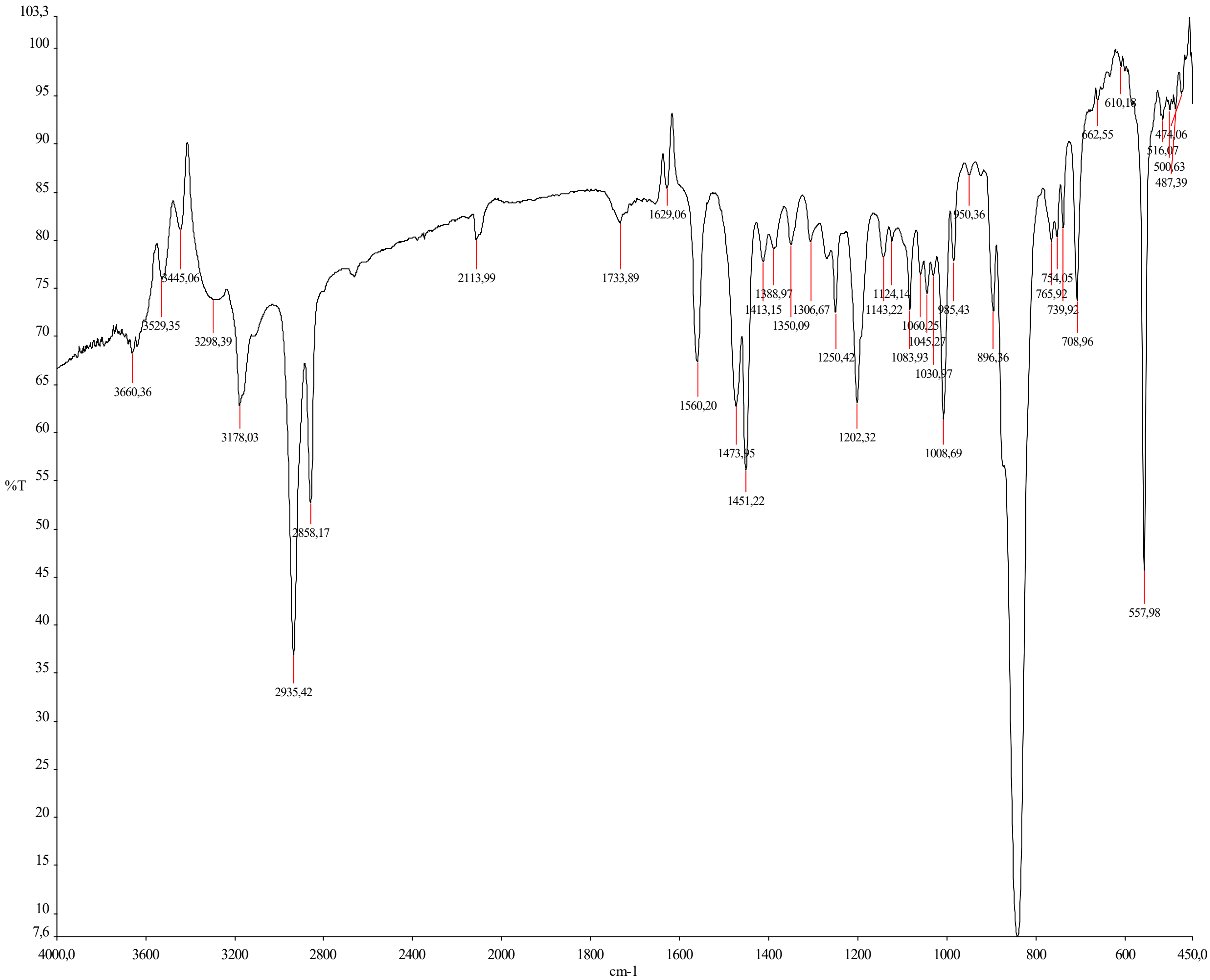

Fig. S18. FT-IR spectrum (KBr) of [Ru(S_2C·ICy)$_3$](PF_6)$_2$ (**2c**)

Fig. S19. FT-IR spectrum (KBr) of [Ru($S_2C\cdot$SIMes)$_3$](PF_6)$_2$ (**2d**)

Fig. S20. FT-IR spectrum (KBr) of $[Ru(S_2C{\cdot}SIDip)_3](PF_6)_2$ (**2e**)

Part 3 – Mass spectra

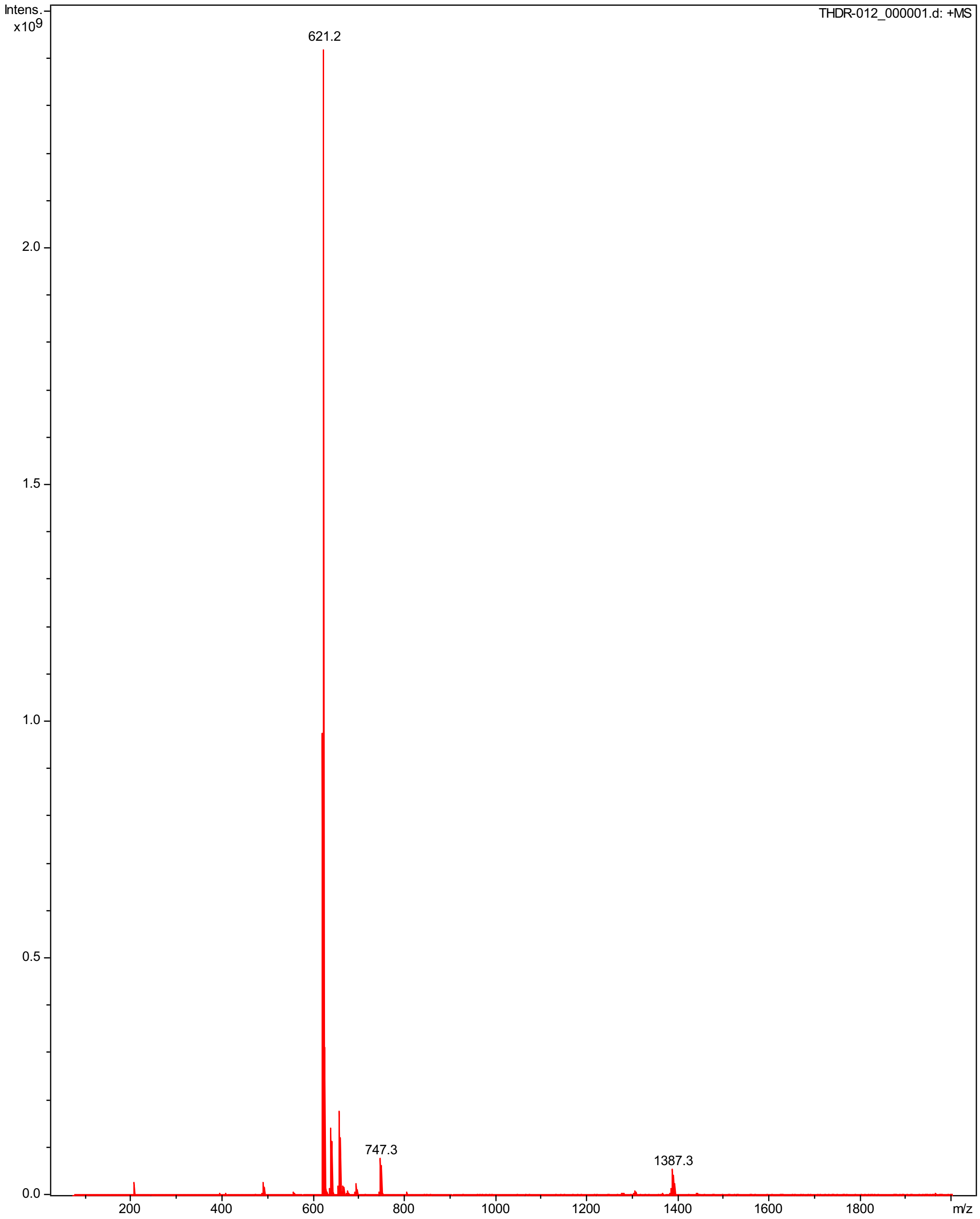

Fig. S21. ESI-MS spectrum of $[Ru(S_2C{\cdot}IMes)_3](PF_6)_2$ (**2a**)

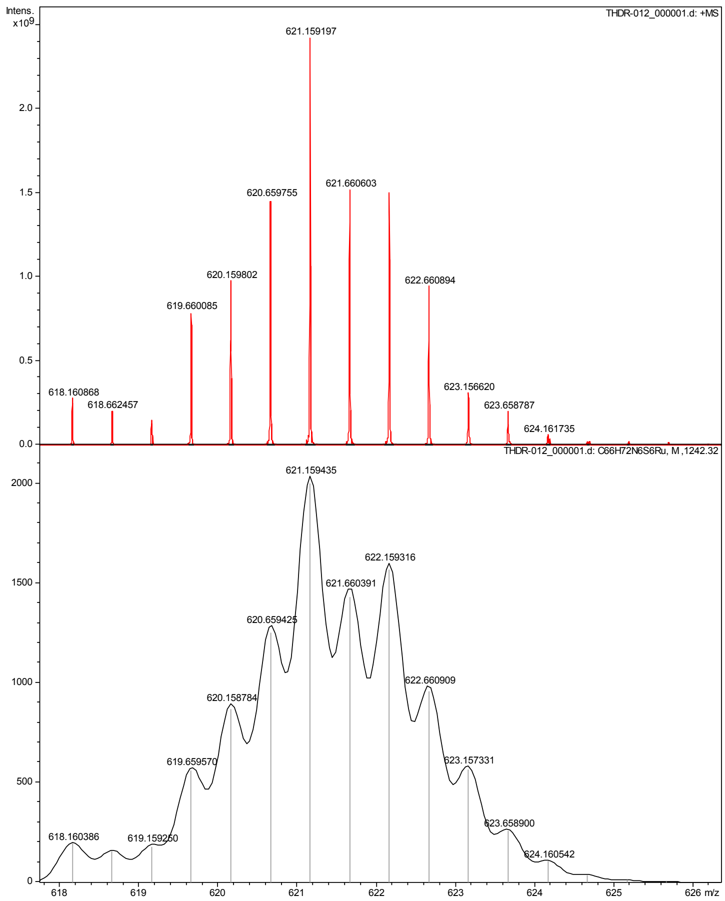

Fig. S22. Isotope profiles of $[Ru(S_2C{\cdot}IMes)_3]^{2+}$ obtained by ESI-MS (in red) and simulated isotope patterns of the corresponding ion (in black)

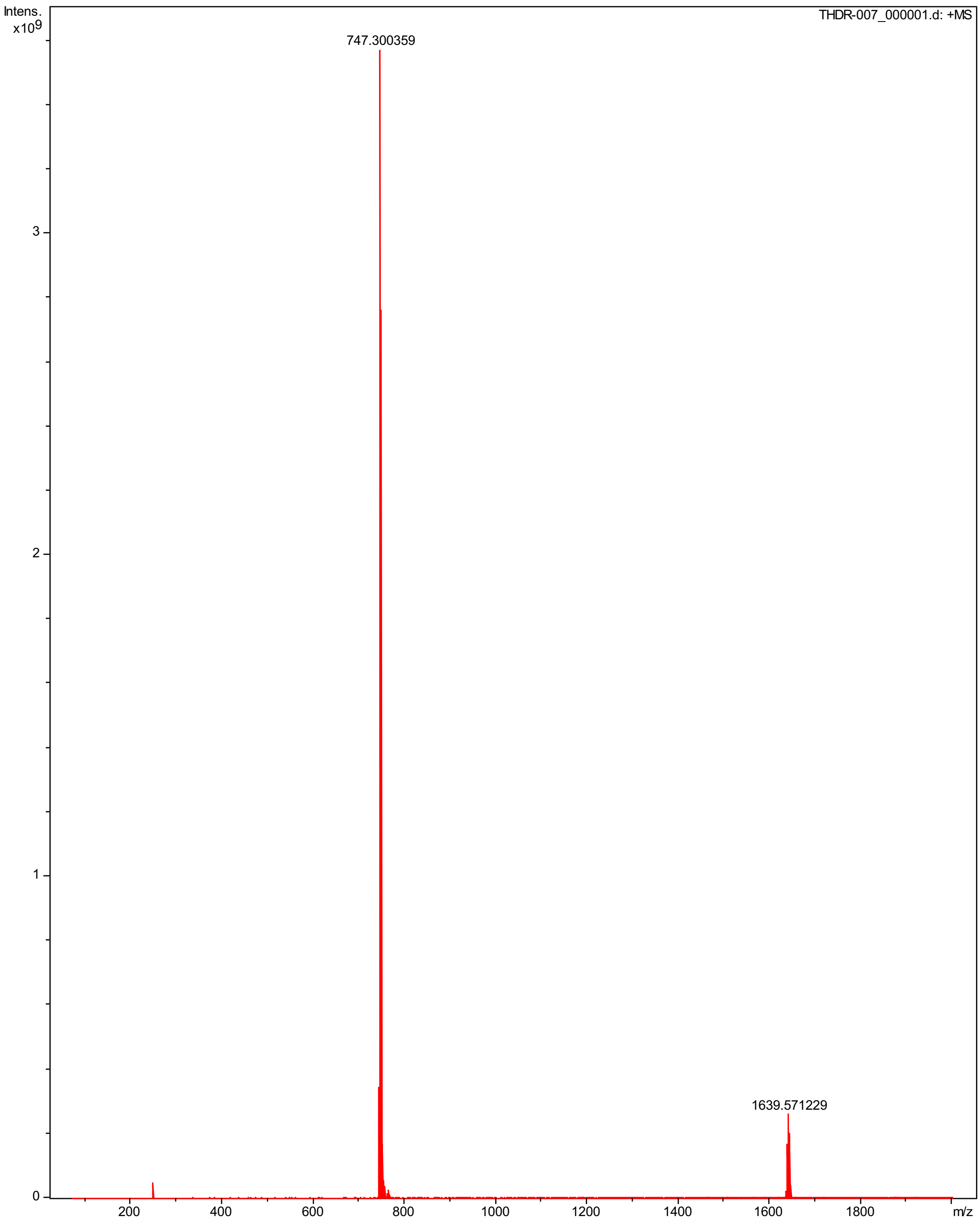

Fig. S23. ESI-MS spectrum of $[Ru(S_2C\cdot IDip)_3](PF_6)_2$ (**2b**)

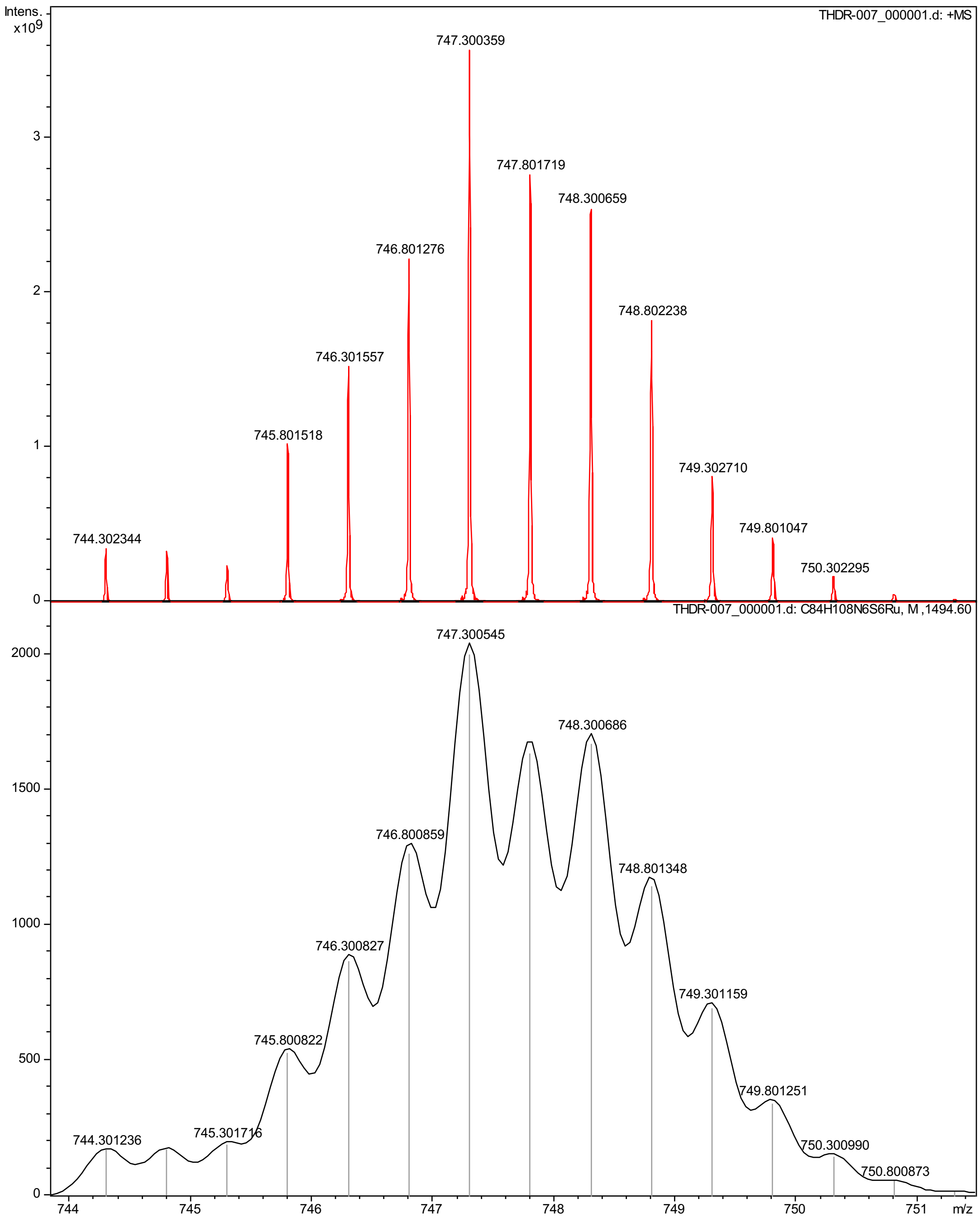

Fig. S24. Isotope profiles of $[Ru(S_2C{\cdot}IDip)_3]^{2+}$ obtained by ESI-MS (in red) and simulated isotope patterns of the corresponding ion (in black)

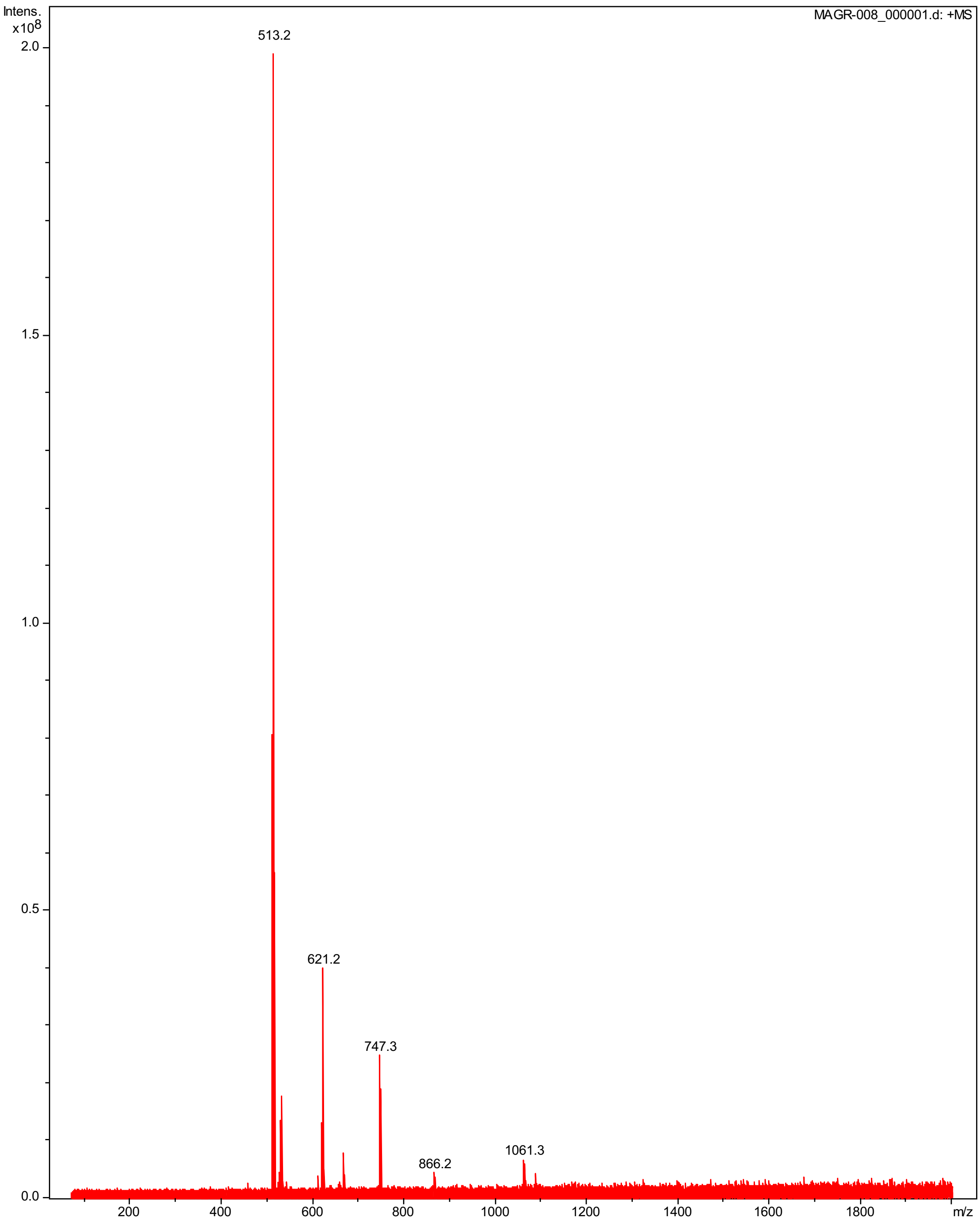

Fig. S25. ESI-MS spectrum of $[Ru(S_2C{\cdot}ICy)_3](PF_6)_2$ (**2c**)

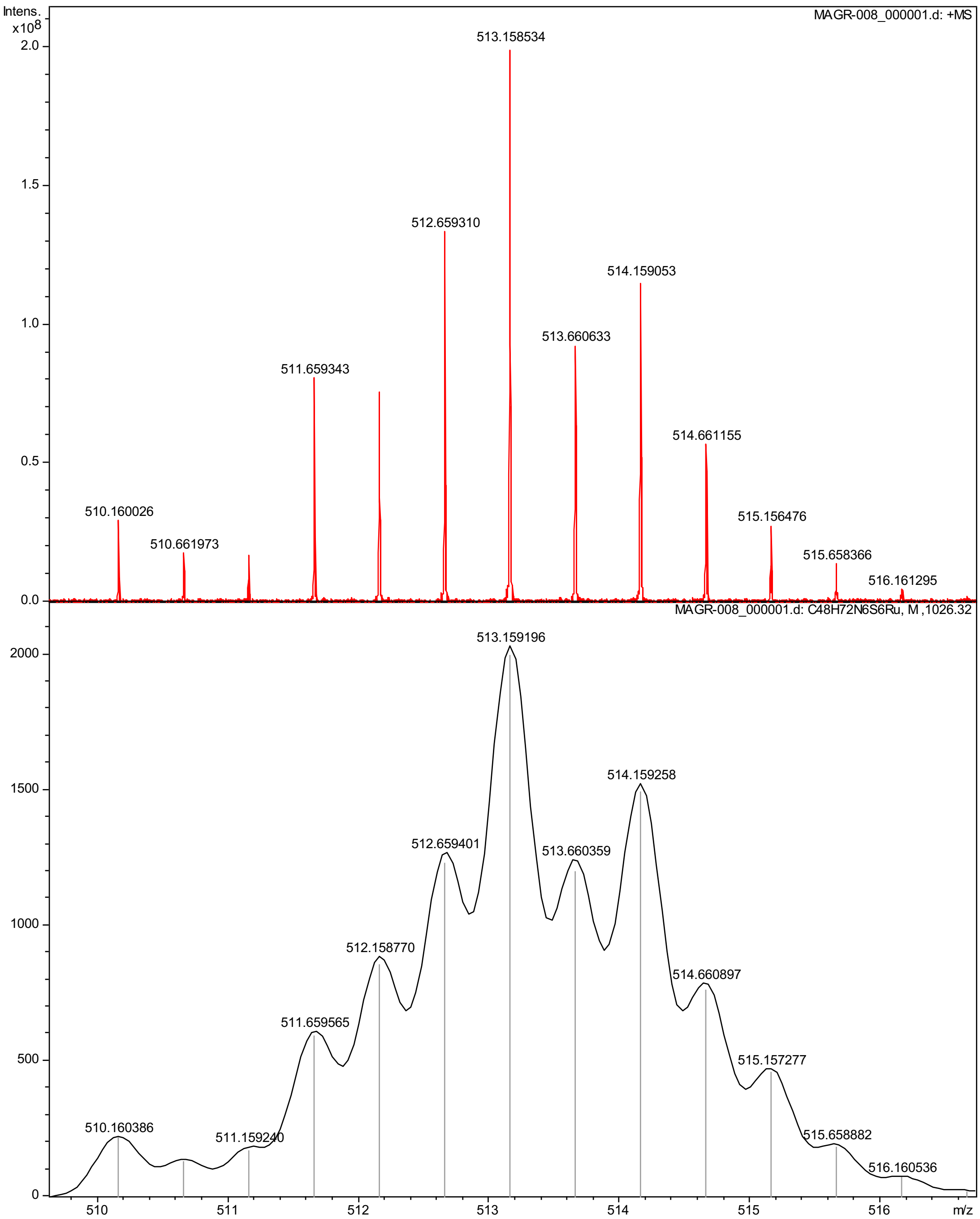

Fig. S26. Isotope profiles of $[Ru(S_2C{\cdot}ICy)_3]^{2+}$ obtained by ESI-MS (in red) and simulated isotope patterns of the corresponding ion (in black)

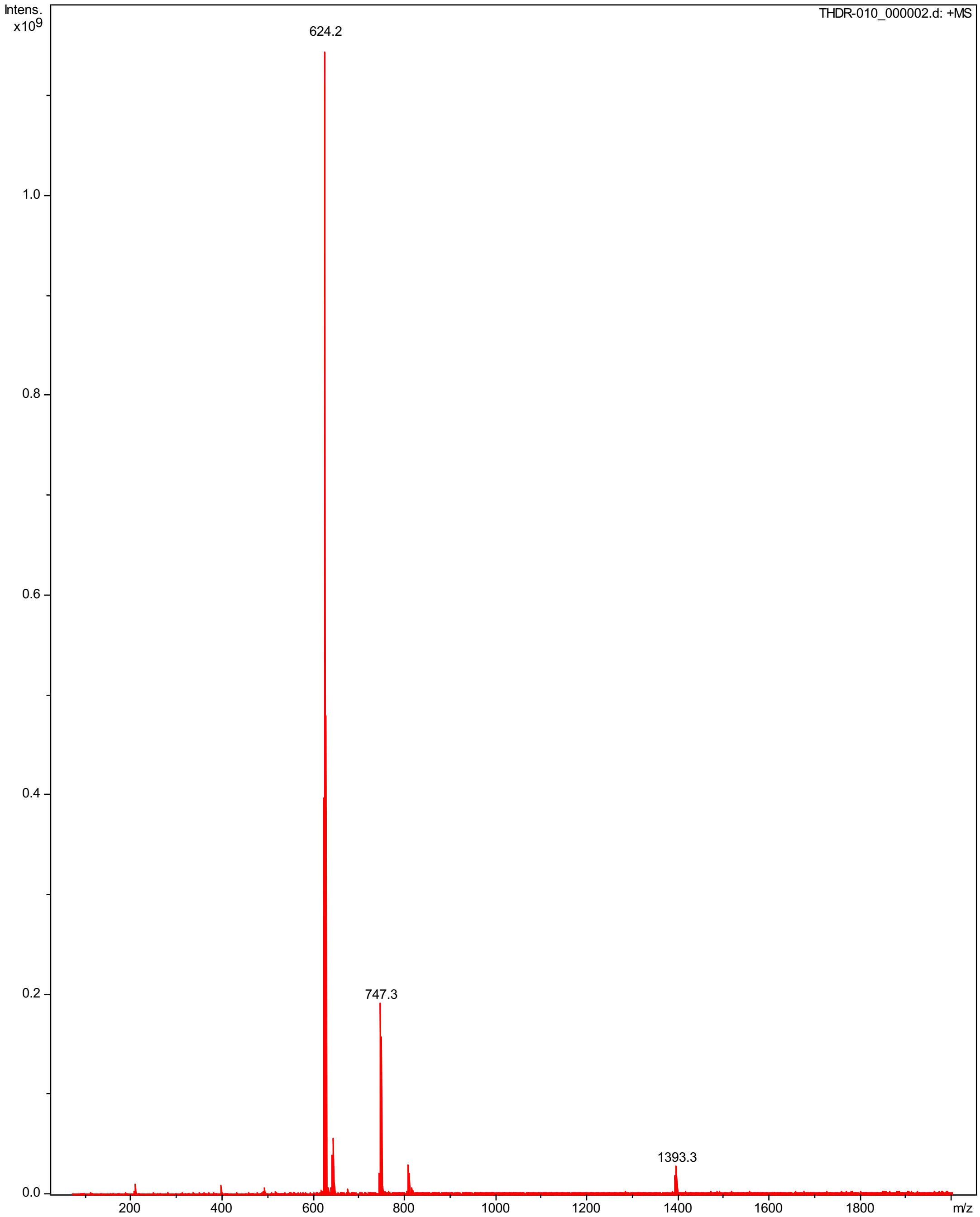

Fig. S27. ESI-MS spectrum of $[Ru(S_2C\cdot SIMes)_3](PF_6)_2$ (**2d**)

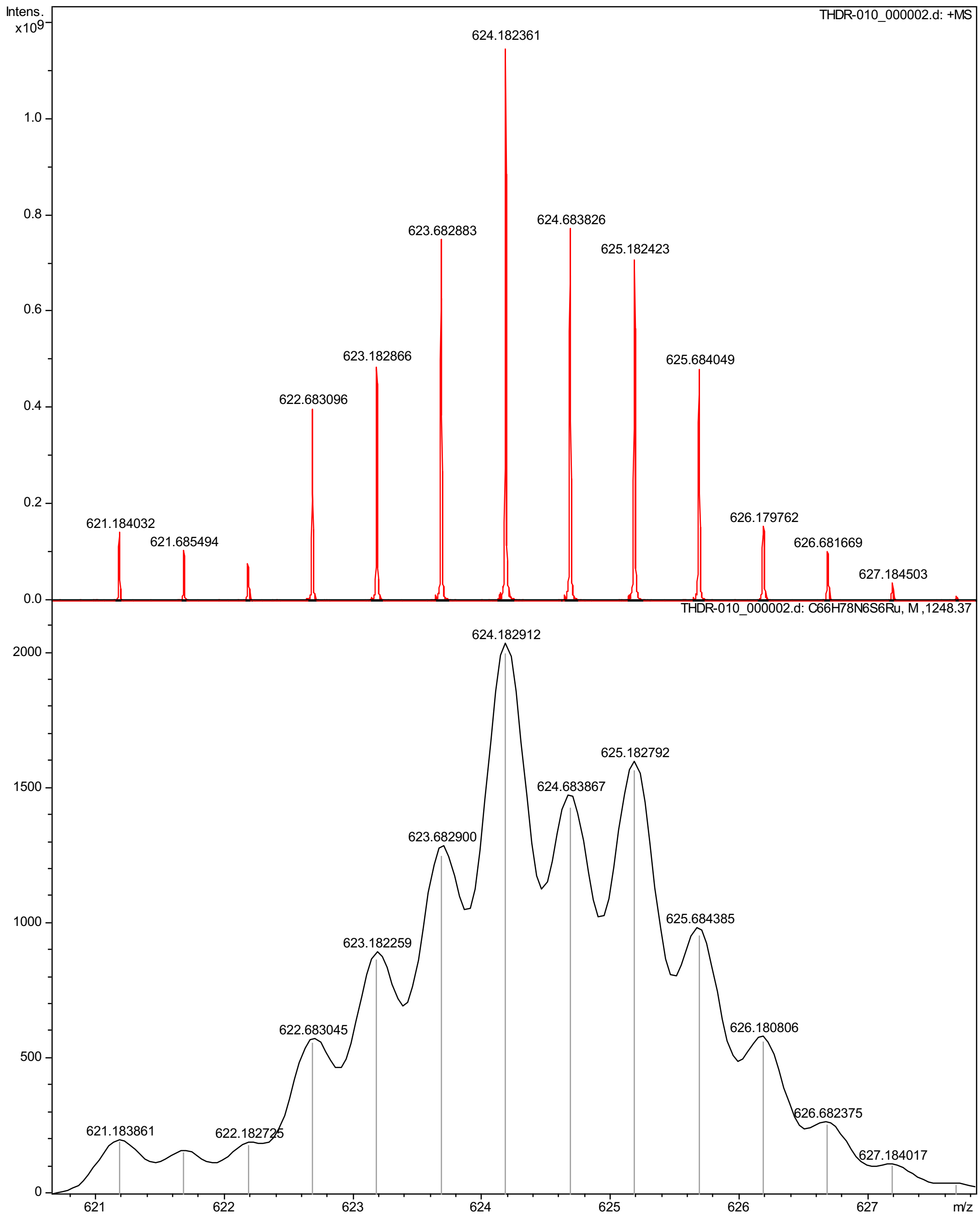

Fig. S28. Isotope profiles of $[Ru(S_2C{\cdot}SIMes)_3]^{2+}$ obtained by ESI-MS (in red) and simulated isotope patterns of the corresponding ion (in black)

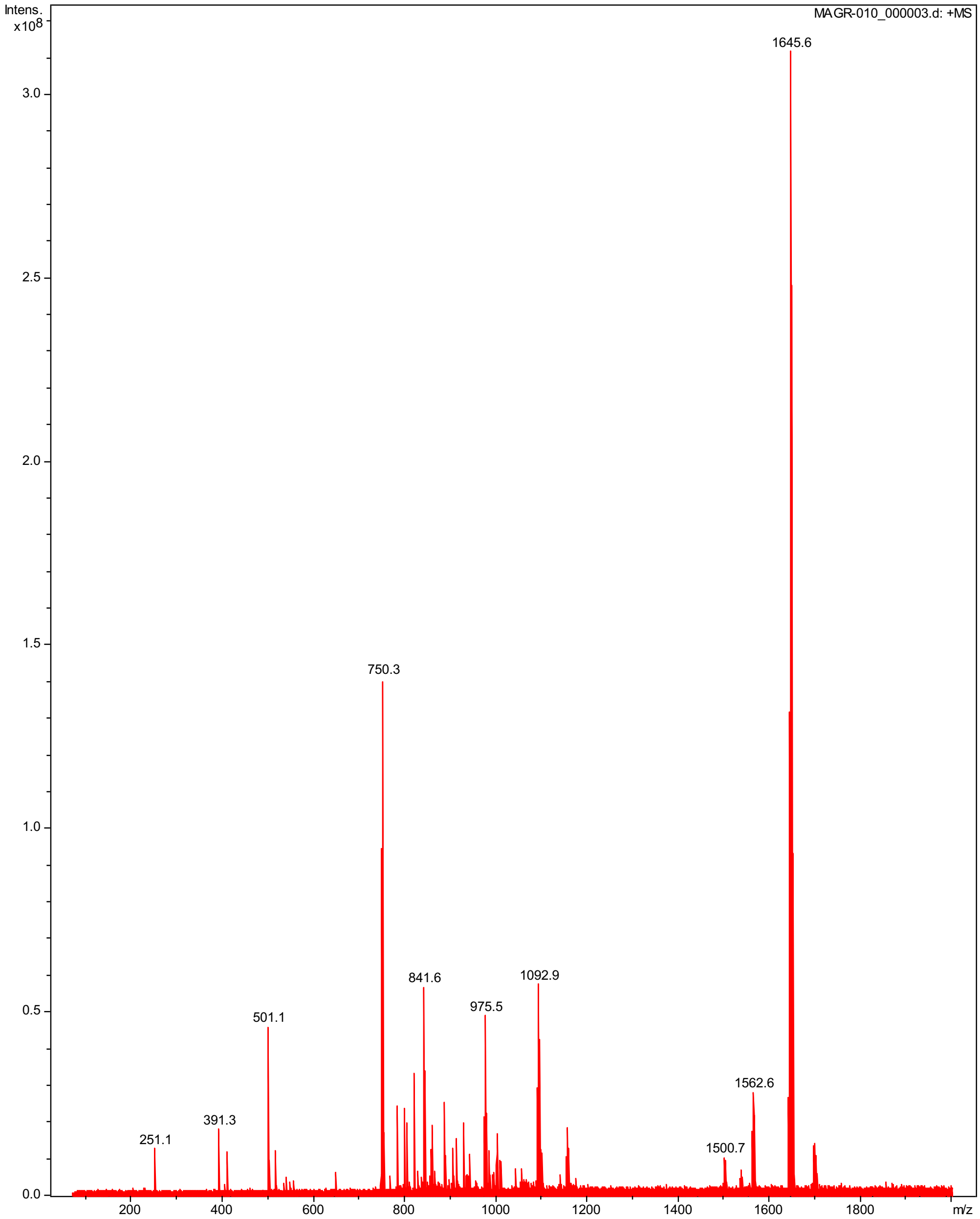

Fig. S29. ESI-MS spectrum of $[Ru(S_2C{\cdot}SIDip)_3](PF_6)_2$ (**2e**)

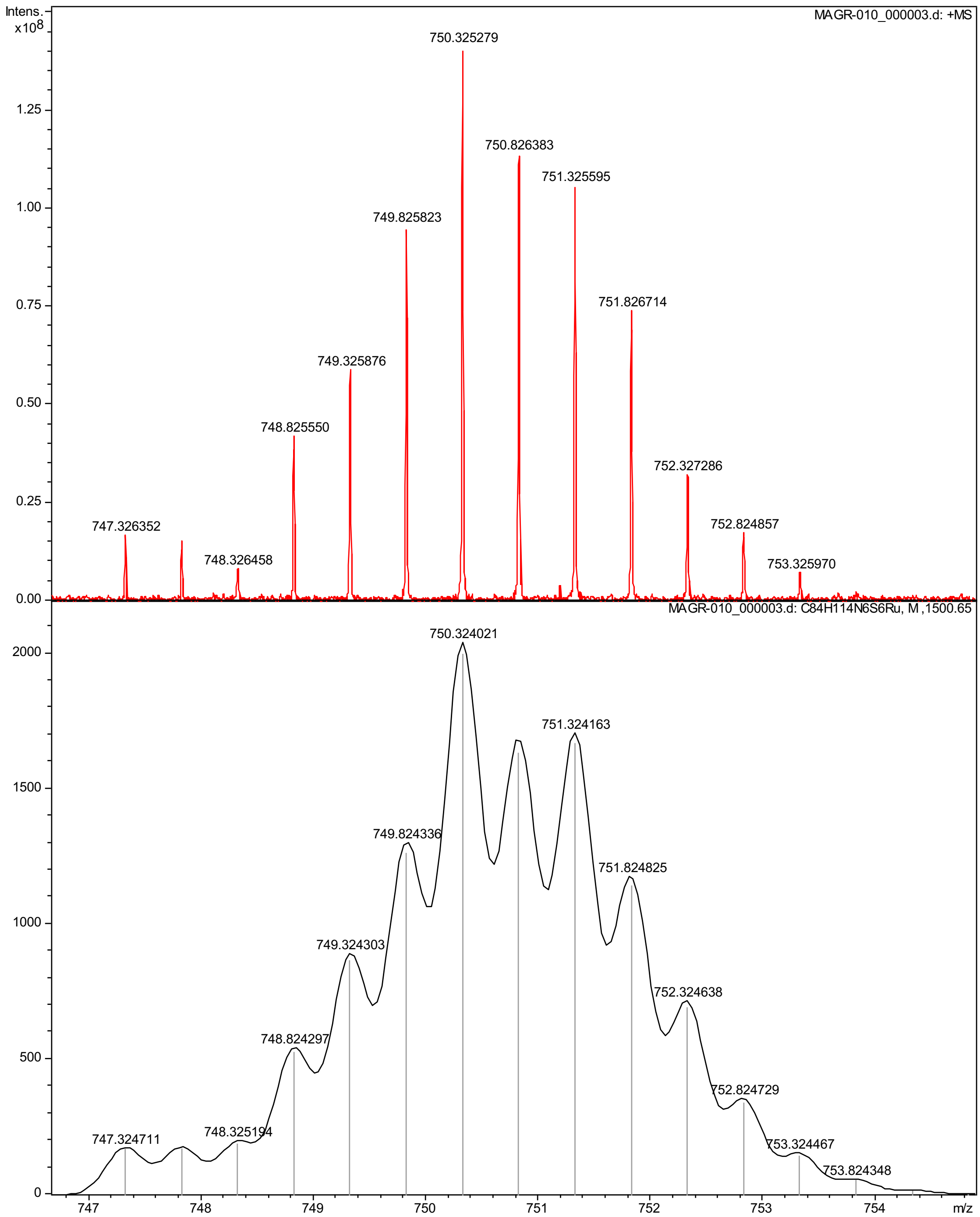

Fig. S30. Isotope profiles of $[Ru(S_2C{\cdot}SIDip)_3]^{2+}$ obtained by ESI-MS (in red) and simulated isotope patterns of the corresponding ion (in black)

Part 4 – Cyclic voltammetry

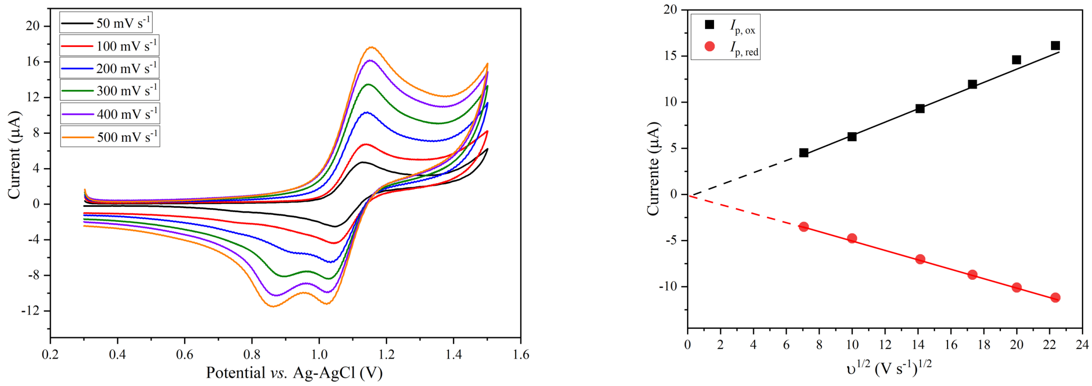

Fig. S31. *Left* - Cyclic voltammograms of $[Ru(S_2C{\cdot}IMes)_3](PF_6)_2$ (**2a**) in CH_2Cl_2 at 25 ºC, scanning anodically at scan rates of 50, 100, 200, 300, 400 and 500 mV s^{-1} ([Ru] = 1.0 mM, [n-Bu_4NPF_6] = 0.1 M). *Right* - Current (I) of the anodic ($I_{p,ox}$) and cathodic ($I_{p,red}$) processes *vs.* square root of the potential scan rate (υ).

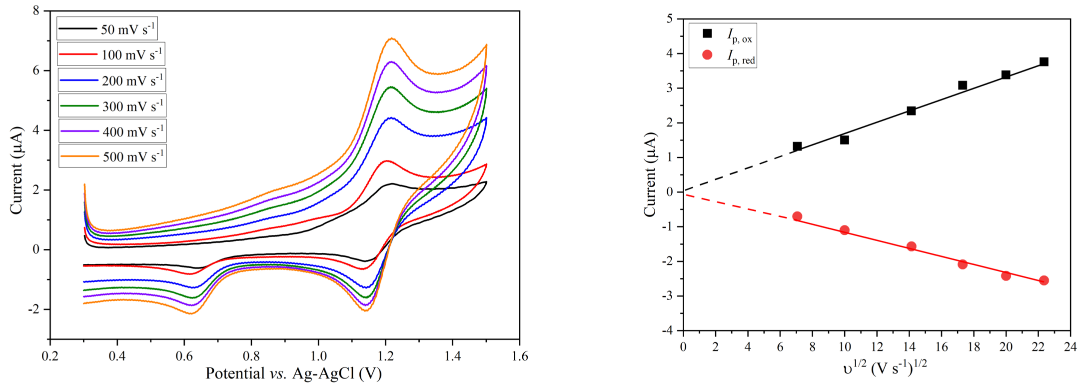

Fig. S32. *Left* - Cyclic voltammograms of $[Ru(S_2C{\cdot}IDip)_3](PF_6)_2$ (**2b**) in CH_2Cl_2 at 25 ºC, scanning anodically at scan rates of 50, 100, 200, 300, 400 and 500 mV s^{-1} ([Ru] = 1.0 mM, [n-Bu_4NPF_6] = 0.1 M). *Right* - Current (I) of the anodic ($I_{p,ox}$) and cathodic ($I_{p,red}$) processes *vs.* square root of the potential scan rate (υ).

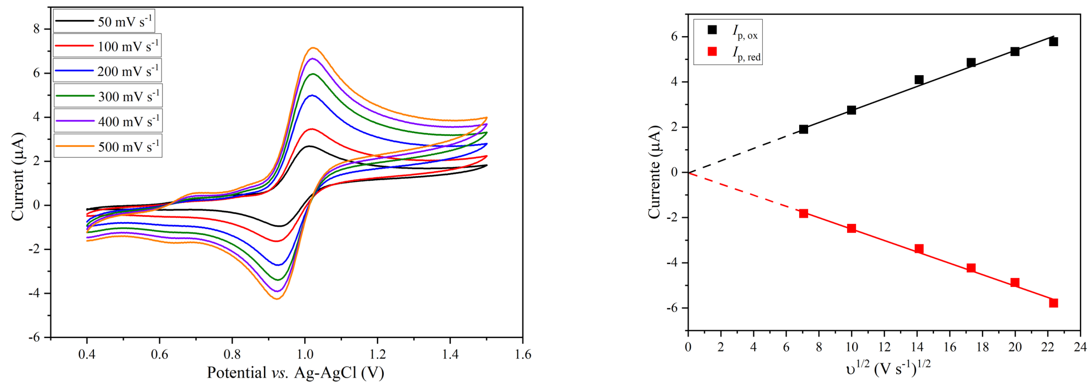

Fig. S33. *Left* - Cyclic voltammograms of $[Ru(S_2C{\cdot}ICy)_3](PF_6)_2$ (**2c**) in CH_2Cl_2 at 25 ºC, scanning anodically at scan rates of 50, 100, 200, 300, 400 and 500 mV s^{-1} ([Ru] = 1.0 mM, [n-Bu_4NPF_6] = 0.1 M). *Right* - Current (I) of the anodic ($I_{p,ox}$) and cathodic ($I_{p,red}$) processes *vs.* square root of the potential scan rate (υ).

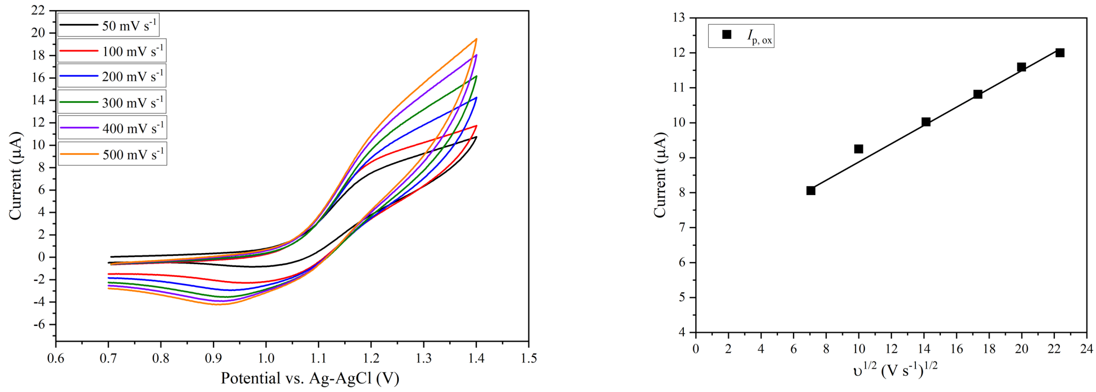

Fig. S34. *Left* - Cyclic voltammograms of $[Ru(S_2C{\cdot}SIMes)_3](PF_6)_2$ (**2d**) in CH_2Cl_2 at 25 ºC, scanning anodically at scan rates of 50, 100, 200, 300, 400 and 500 mV s^{-1} ([Ru] = 1.0 mM, [n-Bu_4NPF_6] = 0.1 M). *Right* - Current (I) of the anodic ($I_{p,ox}$) and cathodic ($I_{p,red}$) processes *vs.* square root of the potential scan rate (υ).

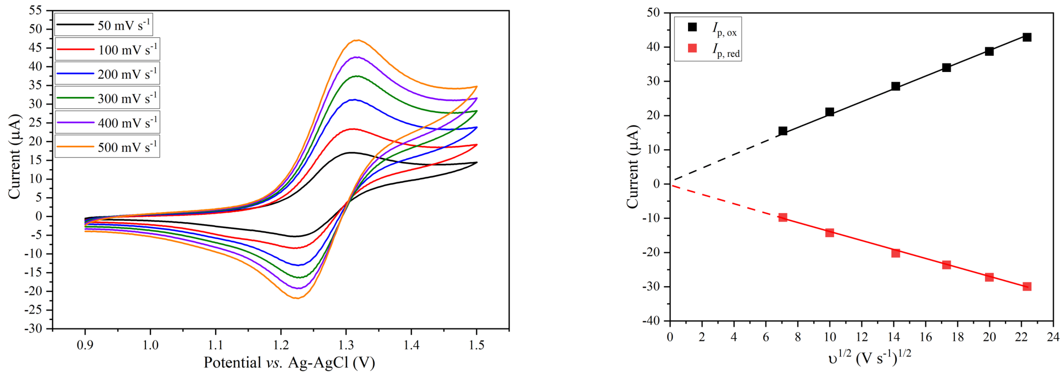

Fig. S35. *Left* - Cyclic voltammograms of $[Ru(S_2C{\cdot}SIMes)_3](PF_6)_2$ (**2e**) in CH_2Cl_2 at 25 ºC, scanning anodically at scan rates of 50, 100, 200, 300, 400 and 500 mV s^{-1} ([Ru] = 1.0 mM, [*n*-Bu_4NPF_6] = 0.1 M). *Right* - Current (*I*) of the anodic ($I_{p,ox}$) and cathodic ($I_{p,red}$) processes *vs.* square root of the potential scan rate (υ).

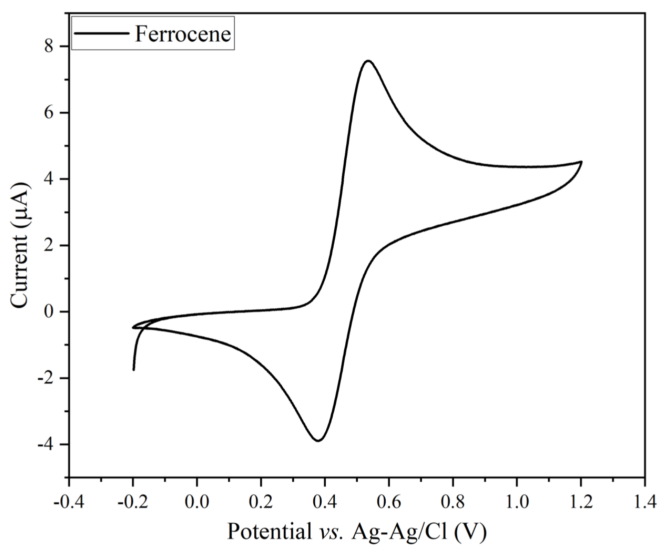

Fig. S36. Cyclic voltammogram of ferrocene in CH_2Cl_2 at 25 ºC, scanning anodically from −0.2 to 1.2 V at scan rate of 100 mV s^{-1} ([Fc] = 1.0 mM, [*n*-Bu_4NPF_6] = 0.1 M).